

Dynamic stimulated emission for deterministic addition and subtraction of propagating photons

Haoyuan Luo,^{1, 2, 3, *} Parth S. Shah,^{4, 5} Frank Yang,^{4, 5} Mohammad Mirhosseini,^{4, 5} and Sahand Mahmoodian^{1, 3, †}

¹*Centre for Engineered Quantum Systems, School of Physics,
The University of Sydney, NSW 2006, Australia*

²*Sydney Quantum Academy, Sydney, NSW, Australia*

³*Institute for Photonics and Optical Sciences (IPOS),*

School of Physics, The University of Sydney, NSW 2006, Australia

⁴*Moore Laboratory of Engineering, California Institute of Technology, Pasadena, California 91125, USA*

⁵*Institute for Quantum Information and Matter,
California Institute of Technology, Pasadena, California 91125, USA*

Photon subtraction and addition are essential non-Gaussian processes in quantum optics, where conventional methods using linear optics and number-resolving detection often suffer from low success probability. Here, we introduce the concept of *dynamic stimulated emission*, whereby a quantum emitter undergoes stimulated emission with a time-dependent coupling. We show that, for both two- and three-level emitters, this process can be used to deterministically add or subtract a photon to a single propagating optical mode. We provide semi-analytic solutions to this problem for Fock states, enabling deterministic and unconditional single-photon subtraction and addition with fidelity $\mathcal{F} > 0.996$. Our semi-analytic solutions are provided for both dynamically coupled two-level systems and for three-level systems whose dynamical coupling is controlled by a coherent laser drive. Moving beyond individual Fock states, we further showcase the ability to subtract and add single photons to photon-number superposition states. We show that Schrödinger cat states can be prepared from squeezed vacuum input via cascaded subtraction or cascaded addition. Finally, we show that our photon-addition process can be used to add a photon to any squeezed and displaced state with high success probability and fidelity $\mathcal{F} > 0.99$, thereby potentially converting quantum emitters from single-photon sources to sources of single-photon-added Gaussian states without the need for inline squeezing. Our protocols provide a path towards integrating quantum emitters to construct efficient sources of single-mode non-Gaussian light beyond single photons.

I. INTRODUCTION

Non-Gaussian quantum states of photons are key ingredients for unlocking quantum advantage in continuous-variable quantum computation [1–6], sensing [7, 8], and communication [6, 9, 10]. Exotic non-Gaussian states such as large-photon-number Schrödinger cat states and the Gottesman-Kitaev-Preskill (GKP) state are particularly desired for their error correcting properties [11–13]. While the preparation of these non-Gaussian states has matured in superconducting [13, 14] and trapped ion [15, 16] platforms, they remain elusive in optical systems. Conventional approaches typically rely on feeding squeezed states into linear optical circuits with photon-number-resolving detection acting both as a heralding signal and as the only non-Gaussian operation. These protocols typically have low success probabilities and can be very sensitive to photon loss [17–23].

The two-level transition of a quantum emitter enables the generation of non-Gaussian states of light. For example, when strongly coupled to a single mode, quantum emitters are excellent single-photon sources [24–29]. However, beyond single-photon generation, few schemes for using quantum emitters for single-mode non-Gaussian

state generation have been proposed. Apart from experimental challenges, this is largely because multi-photon emission processes such as superradiance [30–32] produce states of photons featuring entanglement among many temporal modes [33–35]. This contrasts with most quantum information protocols which require photons to be in a single spatiotemporal mode. Extending the scope of quantum emitters to generate single-mode multi-photon states would position them as strong candidates for introducing non-Gaussian operations in optical systems, thereby have significant impact on the efficiency of generating non-Gaussian states. Here, we emphasize the difference between a multi-mode state and a single-mode state. A general n -photon multi-mode state of a one dimensional photon field can be written as

$$\frac{1}{\sqrt{n!}} \int_{\mathbb{R}^n} d^n \mathbf{x} \alpha(\mathbf{x}) \hat{\mathbf{a}}^\dagger(\mathbf{x}) |0\rangle, \quad (1)$$

where $|0\rangle$ is the vacuum, $d^n \mathbf{x} = dx_1 dx_2 \dots dx_n$, $\hat{\mathbf{a}}^\dagger(\mathbf{x}) = \hat{a}^\dagger(x_1) \hat{a}^\dagger(x_2) \dots \hat{a}^\dagger(x_n)$ are the photon creation operators and $\alpha(\mathbf{x})$ is the n -photon symmetric position wavefunction. In the special case when the wavefunction is separable, $\alpha(\mathbf{x}) = f(x_1) \dots f(x_n)$, the state is single-moded with mode function, $f(x)$, and the state is referred to as an n -photon Fock state. Furthermore, scattering a multi-photon Fock state off a quantum emitters generally results in a multi-mode state [36–38].

The goal of this work is to produce transitions between Fock states of different photon-number using quantum

* haoyuan.luo@sydney.edu.au

† sahand.mahmoodian@sydney.edu.au

emitters, in other words, we aim to perform addition and subtraction of single-photons to and from multi-photon Fock states, i.e. $|n-1\rangle \leftrightarrow |n\rangle$. While this is straightforward in the Jaynes-Cummings model, it is a challenging problem for propagating photons. Lund *et al.* presented an appealing solution to this problem by scattering the n -photon Fock state with a passive two-level system (TLS) [39]. But the proposed solution required a fixed relationship between the temporal-mode width and the emitter's coupling strength, and most crucially, it requires the use of quantum pulse gates for multiplexing, which itself is experimentally challenging [40].

In a seminal work, Cirac, Zoller, Kimble, and Mabuchi showed that driven three-level quantum emitters provide an effective dynamic coupling that can be used to emit and absorb single-photons with arbitrary mode shapes [41]. This process can be considered as a special case of single-photon addition and subtraction where the respective initial or final state of the photon field is the vacuum state. Unlike the single-excitation scenario, a multi-photon state can induce stimulated emission in a quantum emitter which greatly complicates the problem. When stimulated emission occurs while the quantum emitter is dynamically coupled, we refer to it as *dynamic stimulated emission*. Inspired by Ref. [41], the goal of this work is to find the dynamic coupling strengths, $g(t)$ such that we can achieve deterministic single-photon addition and subtraction using dynamic stimulated emission when the incoming Fock state has arbitrary number of excitations, see Fig. 1. We demonstrate that with a carefully chosen dynamic coupling strength, a quantum emitter can deterministically add a photon to an incoming multi-photon Fock state and the outgoing state remains in a Fock state. The reverse process occurs when a quantum emitter is excited by an incoming multi-photon Fock state.

In this work, we show that the unconditional fidelities for both the addition and subtraction processes using dynamic stimulated emission with a TLS are $\mathcal{F} > 0.996$. Moreover, in optical experiment settings, an effective TLS with time-dependent coupling can be realised using a far-detuned three-level system (3LS) with the dynamic coupling controlled by a coherent laser drive. We show that the unconditional fidelities when using 3LSs for addition and subtraction of single-photon are $\mathcal{F} > 0.996$. Moving to more general superposition of Fock states, we implement cascaded photon addition and subtraction on squeezed vacuum to prepare high-fidelity Schrödinger cat states. Finally, we show that dynamic stimulated emission has the potential to transform single-photon sources – which add a single photon to vacuum – to sources of photon-added Gaussian states, where a photon is added to a squeezed displaced state. These states can be generated with success probability greater than 0.54 and fidelity $\mathcal{F} > 0.99$.

This article is organized as follows, Sec. II B reviews the dynamic-coupling solution for the addition and subtraction of single-photon using a TLS. In Sec. II C we derive

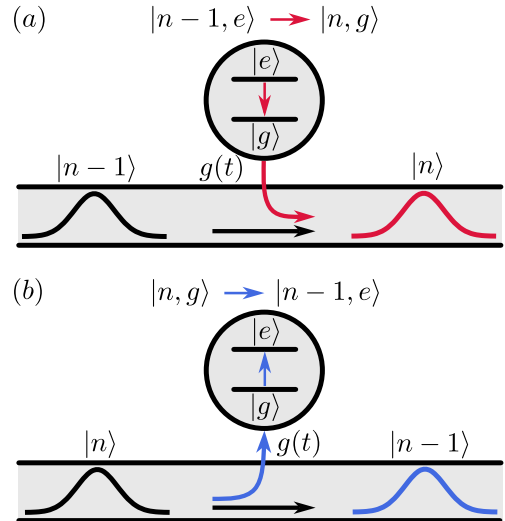


FIG. 1. (a) Schematic of dynamic stimulated emission for the addition of a single-photon to produce an n -photon Fock state in a one-dimensional waveguide QED system. When a $(n-1)$ -photon Fock state pulse is incident on a two-level system (TLS) prepared in the excited state, a carefully chosen dynamic coupling strength $g(t)$ enables the TLS to emit a photon such that output is a n -photon Fock state. (b) Conversely, the schematic of the reverse process (subtraction). The TLS is excited by an n -photon Fock state. The dynamic coupling strengths, $g(t)$ are distinct for each addition and subtraction processes and they dependent on the excitation number and the input mode shape; explicit expressions are given by Eq. (29) and Eq. (28).

the two-excitation solution and present the general solution to an arbitrary number of excitations in Sec. II D. In Sec. II E we discuss the results of addition and subtraction of up to five excitations and cascade up to five TLSs for transitions between Fock states. In Sec. III, we present our solution for using 3LSs for the addition and subtraction of Fock states and the results are discussed in Sec. III C. In Sec. IV A, we cascade TLSs to produce Schrödinger cat states and in Sec. IV A we use dynamic stimulated emission to generate photon-added Gaussian states. We provide concluding remarks in Sec. V.

II. DYNAMIC STIMULATED EMISSION AND ABSORPTION USING TWO-LEVEL SYSTEMS

The problem of single-photon addition and subtraction has been studied extensively and has been solved using Heisenberg's equations [41, 42] and quantum stochastic differential equations [43, 44]. It was shown that, with a dynamic coupling, a quantum emitter can be used to absorb or emit a single photon with any reasonable temporal mode shape. These processes constitute dynamic emission and absorption of a single photon, where respectively, a photon is added to vacuum or a photon is absorbed leaving only vacuum. Here, we extend the pho-

ton addition and subtraction processes to an arbitrary number of excitations, i.e., we extend dynamic emission and absorption to dynamic stimulated emission and absorption. The ideal photon subtraction process for a Fock state is illustrated in Fig. 1(a). This shows a propagating n -photon Fock state in a given temporal mode interacting with a TLS subject to the tailored dynamic coupling rate $g(t)$. The TLS perfectly absorbs one photon and transits to the excited state while the transmitted $(n-1)$ -photon state remains in a single temporal mode. The output temporal mode may be identical to the input mode, but the key requirement is that it remains in a single mode. Since photon subtraction is deterministic and the input and output states are Fock states, the reverse process is the ideal photon addition process, illustrated by Fig. 1(b).

Here, we provide a semi-analytic solution for the dynamical coupling required to implement these ideal addition and subtraction processes for arbitrary input pulse shapes. Our approach can be summarized as follows: start with the most general ansatz for each n -excitation subspace, solve the Schrödinger equation with the known input state and the desired output conditions, then explicitly find the required dynamic coupling strength, $g(t)$. Although the coupling, $g(t)$ for the single-excitation subtraction and addition processes can be solved exactly, it is intractable with an arbitrary number of excitations. Therefore, we perform an effective linearisation of the solution to the Schrödinger equation before solving for the couplings. The linearised solution has a form similar to the single excitation solution, and serves as a starting point for a variational ansatz. This provides a semi-analytic form that achieves near-unit fidelity for arbitrary excitation number.

In this section, we introduce the model before revisiting the single-excitation solution. We follow this by solving the Schrödinger equation for the two-excitation subtraction process, and then introduce the linearisation step before solving for the dynamic coupling strength explicitly. Using induction, we obtain the couplings for the n -excitation subtraction processes. We show that, under time and parity reversal, the couplings for the n -excitation addition processes can be obtained from the subtraction couplings. Lastly, we showcase the results using numerical simulations.

A. Model and background

We begin by considering a two-level system (TLS) coupled with a time-dependent coupling strength to a one-dimensional continuum of right-propagating photons under the dipole, rotating-wave, and Markov approximations. After renormalizing the frequency of the TLS, assuming it to be positioned at $x = 0$, and setting the group velocity to $v_g = \hbar = 1$, the Hamiltonian reads,

$$\hat{H}(t) = -i \int_{\mathbb{R}} dx \hat{a}^\dagger(x) \partial_x \hat{a}(x) + g(t) \hat{\sigma}_+ \hat{a}(0) + \text{h.c.} \quad (2)$$

Here, $\hat{a}(x)$ ($\hat{a}^\dagger(x)$) is the photon annihilation (creation) operator at position x , $\hat{\sigma}_-$ ($\hat{\sigma}_+$) is the Pauli lowering (raising) operator of the TLS, and h.c. indicates the Hermitian conjugate of the preceding term. The first term in the Hamiltonian generates propagation of the photons to the right, while the second and third terms describe the interaction between the TLS and the photon field. The unidirectional coupling is the signature of chiral waveguide QED (quantum electrodynamics) systems [31, 36, 45–48]. In the interaction picture with respect to the free-propagation term, the wavefunction evolution is described by the Hamiltonian,

$$\hat{H}_I(t) = g(t) \hat{\sigma}_+ \hat{a}(-t) + g^*(t) \hat{a}^\dagger(-t) \hat{\sigma}_-. \quad (3)$$

In this co-moving frame and with local interactions, one can interpret the TLS as a boundary that is moving to the left from $x = 0$ to $x = -t$, while interacting with the photon field with coupling strength $g(t)$.

B. Single excitation

Let us review the derivation of the dynamic coupling strength $g(t)$ by solving the Schrödinger equation such that the TLS either absorbs or emits a single photon in a given temporal mode. Since the total number of excitation is conserved, the dynamics are entirely contained in the single-excitation subspace which is captured by the interaction-picture ansatz,

$$|\psi(t)\rangle = \int_{\mathbb{R}} dx \alpha(x, t) \hat{a}^\dagger(x) |0, g\rangle + \beta(t) |0, e\rangle. \quad (4)$$

Here, $|0, i\rangle = |0\rangle \otimes |i\rangle$ is the product state of the vacuum state of the one-dimensional continuum and the ground ($i = g$) or excited ($i = e$) state of the TLS, $\alpha(x, t)$ and $\beta(t)$ are the corresponding wavefunction amplitudes. At all times, they satisfy the normalisation condition, $\int_{\mathbb{R}} dx |\alpha(x, t)|^2 + |\beta(t)|^2 = 1$. From the Schrödinger equation, the equations of motion are,

$$i\partial_t \alpha(x, t) = \delta(x + t) g^*(t) \beta(t), \quad (5)$$

$$i\partial_t \beta(t) = g(t) \alpha(-t, t). \quad (6)$$

We highlight that the $-t$ argument arises as it corresponds to the x coordinate of the TLS in the interaction picture at time t . Before solving these differential equations, let us adapt the language of input–output theory by labeling the single-photon wavefunction $\alpha(x, t)$ in two different regions corresponding to before and after interacting with the TLS,

$$\alpha(x, t) = \begin{cases} \alpha_0(x, t), & x \leq -t \\ \alpha_1(x, t), & x \geq -t \end{cases} \quad (7)$$

since the TLS is moving at position $-t$, then $\alpha_0(x, t)$ and $\alpha_1(x, t)$ are the wavefunctions to the left and right of the TLS. When evaluated at $x = -t$, $\alpha_0(-t, t)$ and $\alpha_1(-t, t)$

are the input and output wavefunctions, respectively. Since Eq. (5) contains a δ -function, we must impose a regularisation condition, $\alpha(-t, t) = [\alpha_0(-t, t) + \alpha_1(-t, t)]/2$, for the single-photon wavefunction evaluated at the position of the TLS [31, 49].

Integrating Eq. (5) in a region away from the position of the photon gives $\alpha(x, t) = \alpha(x, t')$ for $-x \notin [t', t]$. Physically, this means that the wavefunction is constant in the absence of interaction. Alternatively, in the original picture, this implies that the photon freely propagates before and after the scattering process. This allows us to relate the photon input wavefunction to the initial state by $\alpha_0(-t, t) = \alpha_0(-t, 0)$. On the other hand, integrating over the position of the photon produces the boundary condition or equivalently, the single-excitation input-output relation,

$$\alpha_1(-t, t) - \alpha_0(-t, t) = -ig^*(t)\beta(t). \quad (8)$$

With the regularisation condition and the boundary condition, Eq. (6) becomes a differential equation for the wavefunction of the excited state population, $\partial_t\beta(t) = -|g(t)|^2\beta(t)/2 - ig(t)\alpha_0(-t, 0)$. The solution to this is

$$\beta(t) = e^{-\frac{G(0,t)}{2}} \left[\beta(0) - i \int_0^t dt' g(t') e^{\frac{G(0,t')}{2}} \alpha_0(-t', 0) \right], \quad (9)$$

where $G(0, t) = \int_0^t dt' |g(t')|^2$. In the above equation for $\beta(t)$, the exponential factor outside the square brackets is responsible for the decay of the TLS, while the terms on the inside are the initial excited state amplitude and the source term arising from the incoming photon.

To solve for subtraction and addition of a single-photon we must substitute Eq. (9) into the boundary condition Eq. (8), then set the appropriate initial conditions and the desired boundary conditions. For single-photon emission, i.e. addition to vacuum, the goal is to release the excitation from the TLS as a single photon of a specific temporal mode, $f_{\text{out}}(-t)$. Therefore, the initial and boundary conditions are $\beta(0) = 1$, $\alpha(x, 0) = 0$ and $\alpha_0(-t, t) = 0$, $\alpha_1(-t, t) = f_{\text{out}}(-t)$. All together with Eq. (8), we have the single-photon addition boundary condition, $f_{\text{out}}(-t) = -ig^*(t)e^{-G(0,t)/2}$. This equation can be inverted by integrating its squared modulus, $|f_{\text{out}}(-t)|^2 = -\partial_t e^{-G(0,t)}$, and the explicit time-dependent coupling strength reads [43],

$$g_{\text{add},1}^*(t) = \frac{if_{\text{out}}(-t)}{\sqrt{\int_t^\infty dt' |f_{\text{out}}(-t')|^2}}. \quad (10)$$

Here, the subscript denotes that it is a tailored dynamic coupling for the single-excitation addition process. Conversely, the process of single-photon absorption is when a photon in the temporal mode $f_{\text{in}}(-t)$ is completely absorbed and excites the TLS which remains in $|e\rangle$. Here, the initial and boundary conditions are $\beta(0) = 0$, $\alpha_0(x, 0) = f_{\text{in}}(x)$, $\alpha_1(x, 0) = 0$ and $\alpha_0(-t, t) = f_{\text{in}}(-t)$, $\alpha_1(-t, t) = 0$ i.e., we require no photon to be transmit-

ted. Substituting these conditions into Eq. (8), we obtain the single-photon subtraction boundary condition, $f_{\text{in}}(-t) = g^*(t)e^{-G(0,t)/2}S_{1/2}(0, t)$, where

$$S_v(a, b) = \int_a^b dt' g(t') e^{vG(a,t')} f_{\text{in}}(-t'), \quad (11)$$

is the source term to excite the TLS in the time interval $[a, b]$ with $v \in \mathbb{C}$. The physical interpretation behind the product of $S_{1/2}(0, t)$ and the decay term $g^*(t)e^{-G(0,t)/2}$ is straightforward: the TLS is being excited by a photon in the time interval $[0, t]$, but at the same time the excitation could also decay. The explicit time-dependent coupling strength is given by (see Appendix A) [44],

$$g_{\text{sub},1}^*(t) = \frac{f_{\text{in}}(-t)}{\sqrt{\int_0^t dt' |f_{\text{in}}(-t')|^2}}. \quad (12)$$

C. Two excitations

Now that we have reviewed the single-excitation case, in this subsection, we generalise the subtraction and addition processes to two excitations. Ideal two-excitation addition occurs when the TLS is initially in the excited state and undergoes dynamic stimulated emission to emit a photon to the incoming single-photon Fock state with unit probability. The output two-photon state must then be a Fock state with a separable wavefunction. Conversely, ideal two-excitation subtraction occurs when the TLS absorbs a photon from the input two-photon Fock state with unit probability. Notice that if the subtraction process has unit absorption probability, the output state is automatically a single-photon Fock state. However, the same cannot be said about the addition process, as the TLS could emit a photon with unit probability but the output wavefunction is not guaranteed to be single-moded. Moreover, we emphasize that the output mode does not necessarily have to be the same as the input mode. Solving for the dynamics required for ideal addition and subtraction in the two-excitation counterpart is significantly more difficult than for one excitation due to the nonlinearity of the TLS. Hence, we only explicitly obtain the time-dependent coupling strength after performing a linear approximation. Nevertheless, as we show in Sec. II E, these approximate solutions provide near-unit fidelities.

By the conservation of the total number of excitations, the dynamics is fully captured by the two-excitation ansatz,

$$|\psi(t)\rangle = \frac{1}{\sqrt{2}} \int_{\mathbb{R}^2} dx_1 dx_2 \alpha(x_1, x_2, t) \hat{a}^\dagger(x_1) \hat{a}^\dagger(x_2) |0, g\rangle + \int_{\mathbb{R}} dx \beta(x, t) \hat{a}^\dagger(x) |0, e\rangle. \quad (13)$$

where $\alpha(x_1, x_2, t)$ is the two-photon symmetric wavefunction with the TLS in the ground state, and similarly

$\beta(x, t)$ is the single-photon wavefunction with the TLS in the excited state. These wavefunctions are normalised by $\int_{\mathbb{R}^2} dx_1 dx_2 |\alpha(x_1, x_2, t)|^2 + \int_{\mathbb{R}} dx |\beta(x, t)|^2 = 1$. From the Schrödinger equation, the equations of motion are

$$i\partial_t \alpha(x_1, x_2, t) = \frac{g^*(t)}{\sqrt{2}} [\beta(x_1, t) \delta(x_2 + t) \quad (14)$$

$$+ \beta(x_2, t) \delta(x_1 + t)],$$

$$i\partial_t \beta(x, t) = \sqrt{2}g(t)\alpha(x, -t, t). \quad (15)$$

Restricting the domain to $x_1 \geq x_2$ imposes a position ordering on the two photons, rendering the two-photon wavefunction unsymmetrised. Importantly, this implies that the scattering process becomes *sequential*, allowing us to solve for the wavefunctions in distinct regions defined by the photons' coordinates relative to the TLS. Specifically, we label the wavefunctions in different regions as follows,

$$\alpha_{\text{unsym}}(x_1, x_2, t) = \begin{cases} \alpha_0(x_1, x_2, t), & -t \geq x_1 \geq x_2 \\ \alpha_1(x_1, x_2, t), & x_1 \geq -t \geq x_2 \\ \alpha_2(x_1, x_2, t), & x_1 \geq x_2 \geq -t \end{cases}, \quad (16)$$

$$\beta(x, t) = \begin{cases} \beta_1(x, t), & x \leq -t \\ \beta_2(x, t), & x \geq -t \end{cases}. \quad (17)$$

The interpretation of each labeling is analogous to that of the input-output wavefunctions of the single-excitation problem. In the interaction picture, the TLS is moving to the left at position $-t$, then the subscripts of the two-photon wavefunctions in different regions indicate the number of photons to the right of the TLS, for example, $\alpha_1(x_1, x_2, t)$ is the two-photon wavefunction with the first photon at position x_1 to the right of the TLS and the second photon at position x_2 to the left. Meanwhile, the subscripts of the single-photon wavefunction label which photon has been absorbed by the TLS, for example, $\beta_1(x, t)$ is the single-photon wavefunction with the first photon absorbed while the second photon is at position x that is to the left of the TLS.

Again, we must impose regularisation conditions for the two-photon wavefunction when either one of the photons is evaluated at the position of the TLS: the unsymmetrical two-photon wavefunction is the average of the wavefunctions in neighbouring regions [31, 49], i.e. $\alpha_{\text{unsym}}(-t, x, t) = [\alpha_0(-t, x, t) + \alpha_1(-t, x, t)]/2$ and similarly, $\alpha_{\text{unsym}}(x, -t, t) = [\alpha_1(x, -t, t) + \alpha_2(x, -t, t)]/2$. Furthermore, The two-photon wavefunction is constant in the absence of interaction i.e., if $-x_1, -x_2 \notin [t', t]$, then $\alpha_{\text{unsym}}(x_1, x_2, t) = \alpha_{\text{unsym}}(x_1, x_2, t')$. On the other hand, the effects of the interaction on the wavefunctions can be seen by integrating Eq. (14) over the position of the photons; which produces the boundary conditions relating the neighboring regions of the two-photon wavefunctions

and the single-photon wavefunctions

$$\alpha_1(-t, x_2, t) - \alpha_0(-t, x_2, t) = \frac{-ig^*(t)}{\sqrt{2}} \beta_1(x_2, t), \quad (18)$$

$$\alpha_2(x_1, -t, t) - \alpha_1(x_1, -t, t) = \frac{-ig^*(t)}{\sqrt{2}} \beta_2(x_1, t). \quad (19)$$

Moreover, since Eq. (15) does not contain a δ -function, the single-photon wavefunctions in different regions match on the boundary, i.e. $\beta_1(-t, t) = \beta_2(-t, t)$.

We proceed by solving for the unknown wavefunctions in the sequence of the photons' coordinates. Specifically, we first solve for the single-photon wavefunction, $\beta_1(x_2, t)$. With the boundary condition in Eq. (18), we relate the two-photon wavefunction, $\alpha_1(x_1, x_2, t)$ to the initial conditions. Repeating the process, we solve for the single-photon wavefunction in the next region, $\beta_2(x_1, t)$, and with Eq. (19), we can express the output two-photon wavefunction, $\alpha_2(x_1, x_2, t)$ in terms of the initial conditions.

By combining the regularisation and the boundary conditions, Eq. (15) produces differential equations for the single-photon wavefunctions, $\partial_t \beta_1(x_2, t) = -|g(t)|^2 \beta_1(x_2, t)/2 - i\sqrt{2}g(t)\alpha_0(-t, x_2, 0)$ and $\partial_t \beta_2(x_1, t) = -|g(t)|^2 \beta_2(x_1, t)/2 - i\sqrt{2}g(t)\alpha_1(x_1, -t, -x_1)$. Depending on the initial condition, the $\beta_1(x_2, t)$ equation describes the dynamics of the arrival or the emission of the first photon in the domain, $t \in [0, -x_1]$. While the $\beta_2(x_1, t)$ equation describes the dynamics when a photon has scattered past the TLS and the second photon is incoming, with the corresponding domain, $t \in [-x_1, -x_2]$. Notably, we have taken advantage of the free-propagation of photons by substituting $\alpha_0(-t, x_2, t) = \alpha_0(-t, x_2, 0)$ and $\alpha_1(x_1, -t, t) = \alpha_1(x_1, -t, -x_1)$ into the single-photon wavefunction differential equations. Explicitly, the solution for $\beta_1(x_2, t)$ is

$$\beta_1(x_2, t) = e^{-G(0, t)/2} \left[\beta_1(x_2, 0) - i\sqrt{2} \int_0^t dt' g(t') e^{G(0, t')/2} \alpha_0(-t', x_2, 0) \right]. \quad (20)$$

The dynamics of the TLS are similar to that of the single-excitation case, where the first term inside the square brackets of Eq. (20) corresponds to the decay of any initial excitation of the TLS and constitutes the emission of the first photon at position $-t \geq x_2$. The second term is responsible for exciting the TLS, but only from the first photon. Together with the $\beta_1(x_2, t)$ solution and the boundary condition in Eq. (18), we can completely express $\alpha_1(x_1, x_2, t)$ in terms of the initial conditions. We are now ready to solve the interaction in the next region. Matching the single-photon wavefunctions at the bound-

ary, the solution to the $\beta_2(x_1, t)$ differential equation is,

$$\beta_2(x_1, t) = e^{-G(-x_1, t)/2} \left[\beta_1(x_1, -x_1) - i\sqrt{2} \int_{-x}^t dt' g(t') e^{G(-x_1, t')/2} \alpha_1(x_1, -t', -x_1) \right]. \quad (21)$$

The first term in the square brackets corresponds to the decay of the leftover excitation in the TLS from the previous region, but the emitted photon is instead the second photon as the first photon is to the right of the TLS at position x_1 . At the same time, the TLS has a chance to be excited by the incoming second photon, this is indicated by the having $\alpha_1(x, -t, -x)$ in the source term. With the boundary condition given by Eq. (19), we can express the output two-photon wavefunction, $\alpha_2(x_1, x_2, t)$ in terms of the initial conditions. We have therefore solved for the dynamics of the system in terms of the initial conditions

and the dynamic coupling coefficient $g(t)$.

We now wish to proceed to determine the dynamic stimulated emission process that enables photon addition, and its reverse process that allows for photon subtraction. This means finding the appropriate dynamical coupling $g(t)$ the enables addition or subtraction. We proceed by first solving the two-excitation subtraction process. The corresponding initial state is,

$$|\psi(t=0)\rangle = \frac{1}{\sqrt{2}} \left[\int_{\mathbb{R}} dx f_{\text{in}}(x) \hat{a}^\dagger(x) \right]^2 |0, g\rangle, \quad (22)$$

with the normalised input mode, $\int_{\mathbb{R}} dx |f_{\text{in}}(x)|^2 = 1$. This initial state corresponds to the initial conditions, $\beta(x, 0) = 0$ and $\alpha_0(x_1, x_2, 0) = f_{\text{in}}(x_1) f_{\text{in}}(x_2)$. For the ideal two-excitation subtraction process, a sufficient condition on the boundary condition is $\alpha_2(x_1, x_2, t) = 0$; hence, Eq. (19) becomes $\alpha_1(x_1, -t, t) = ig^*(t)\beta_2(x_1, t)/\sqrt{2}$. Expressed in terms of the initial condition, the boundary condition reads

$$f_{\text{in}}(-t) B(x_1) = g^*(t) \left[f_{\text{in}}(x_1) e^{-G(0, t)/2} S_{1/2}(0, -x_1) + B(x_1) e^{-G(-x_1, t)/2} S_{1/2}(-x_1, t) \right]. \quad (23)$$

Here, $B(x) = f_{\text{in}}(x) - g^*(-x) e^{-G(0, -x)/2} S_{1/2}(0, -x)$. Notice that, $B(x) = 0$ is the boundary condition required for the single-excitation subtraction process, indicating that its solution would not satisfy Eq. (23) and fail in two excitations. The ramification is that no dynamic coupling exists such that a TLS is excited by a superposition of single- and two-photon Fock state with unit probability. An intuitive explanation is that the interaction in the single-excitation subspace is linear, and the nonlinearity of the TLS only comes into effect when the excitation number is greater than one. Hence, the single- and two-excitation dynamics are dramatically different, consequently, they do not share a common dynamic coupling for exciting the TLS.

The nonlinear response of the TLS can be examined by pinpointing the contributing terms in Eq. (23). The left-hand side of Eq. (23) is the two-photon wavefunction with a photon on either sides of the TLS; there are two contributing terms, namely, the free propagation term and the interaction term. The former can be seen by the product of the input temporal modes evaluated at different positions, $f_{\text{in}}(-t)f_{\text{in}}(x)$. The latter occurs when the TLS absorbs the first photon in the time interval $[0, -x_1]$ and decays to emit a photon just to the right of the TLS at position x_1 , this is indicated by the product of the decay and the source term, $e^{-G(0, -x_1)/2} S_{1/2}(0, -x_1)$.

Meanwhile, the right-hand side of Eq. (23) is the single-photon wavefunction with a photon to the right of the excited TLS; it consists of a superposition of three different contributing processes. In the order of summation,

1. The first process occurs when the TLS absorbs the first photon in the time interval $[0, -x_1]$, as indicated by the source term, $S_{1/2}(0, -x_1)$. But instead of decaying, the TLS remains in the excited state in the time interval $[0, t]$. The excited TLS allows the second photon to freely propagate past the TLS, as suggested by having the temporal mode evaluated at x_1 . Subsequently, the position ordering of the photons is swapped.
2. The second process, hidden in $B(x_1)$ on the right-hand side of Eq. (23), occurs when the first photon freely propagates and passes the TLS at position x_1 . The TLS is then excited by the second photon in the time interval $[-x_1, t]$, as can be seen by the source term $S_{1/2}(-x_1, t)$.
3. The third process, also hidden in $B(x_1)$, occurs when the TLS absorbs the first photon between the time interval $[0, -x_1]$ then emits a photon at position x_1 and starts to absorb the second photon in the interval $[-x_1, t]$, as indicated by the product, $e^{-G(0, -x_1)/2} S_{1/2}(0, -x_1) e^{-G(-x_1, t)/2} S_{1/2}(-x_1, t)$.

Finding the time-dependent coupling strength $g(t)$ that satisfies Eq. (23) would produce the ideal two-excitation subtraction process. However, Eq. (23) involves $g(t)$ evaluated at different times and integrated between different time intervals, hence it is difficult to find an explicit expression of the coupling strength. Instead, we make a linear approximation that eliminates

the second and the third processes of the right-hand side of Eq. (23) and only the first process remains, which corresponds to the TLS absorbing the first photon while the second photon freely propagates past the TLS. We note that, the position ordering of the photons is merely a consequence of working with the unsymmetrised wavefunction, in actuality, the TLS could be excited by any of the two photons. Then this linear approximation can be understood as the TLS only interacts with one photon from the two-photon field. Moreover, the linear approximation corresponds to setting $x_1 = -t$ in Eq. (23) and it becomes the linearised two-excitation subtraction boundary condition, $f_{\text{in}}(-t) = 2g^*(t)e^{-G(0,t)/2}S_{1/2}(0,t)$, which differs from the boundary condition for the single-photon subtraction process by a multiplicative factor of 2.

Before finding the time-dependent coupling strength that satisfies the linearised boundary condition, we present a more general boundary condition that appears in the n -photon subtraction process in Sec. II D and the three-level system photon subtraction in Sec. III. Together, the general boundary condition and its solution are (see Appendix A)

$$f_{\text{in}}(-t) = ug^*(t) \int_0^t dt' g(t') e^{vG(t,t')} f_{\text{in}}(-t'), \quad (24)$$

$$g^*(t) = \frac{f_{\text{in}}(-t)}{\sqrt{2 \operatorname{Re}(u-v) F(t)^{\frac{u-v}{\operatorname{Re}(u-v)}}}}, \quad (25)$$

where $u, v \in \mathbb{C}$, $\operatorname{Re}(\cdot)$ denotes the real part of a complex number and $F(t) = \int_0^t dt' |f_{\text{in}}(-t')|^2$. From Eq. (25), it is clear that $\operatorname{Re}(u-v) \neq 0$.

Setting $u = 2$ and $v = 1/2$ in Eq. (24) and Eq. (25), we recover the linearised two-excitation subtraction boundary condition and obtain its solution. To check the validity of the linearised solution we derive the output single-photon wavefunction from Eq. (21) by taking the infinite-time limit, $\lim_{t \rightarrow \infty} \beta_2(x, t) = -i\sqrt{\frac{3}{8}} [1 + F(-x)^{2/3}] f_{\text{in}}(x)$. Integrating the squared modulus of the single-photon wavefunction yields the probability of a successful subtraction, $\int_{\mathbb{R}} dx |\lim_{t \rightarrow \infty} \beta_2(x, t)|^2 = 69/70 \approx 0.986$. It is remarkable that the solution obtained from solving the approximate boundary condition can produce such a high probability.

We now make a critical assumption allowing us to construct a variational ansatz: we assume that, if we were to include the nonlinear terms in the solution, they would have a largely similar time-dependence thereby only changing the amplitude of $g(t)$ and preserving its shape. We therefore multiply our linearised solution with a variational parameter, $s_2 \in \mathbb{R}$, here the subscript denotes the excitation number. In terms of Eq. (24), this variation corresponds to solving a slightly different boundary condition. Explicitly, the dynamic coupling strength ansatz for the two-excitation subtraction pro-

cess is,

$$g_{\text{sub},2}^*(t) = \frac{s_2 f_{\text{in}}(-t)}{\sqrt{3 \int_0^t dt' |f_{\text{in}}(-t')|^2}}. \quad (26)$$

After optimising towards unit probability with a Gaussian input temporal mode, the value of the optimised variational parameter is $s_2 = 1.072$, which is *invariant* under changes to the width of the Gaussian. The probability or the fidelity with the optimised parameter for the two-excitation subtraction process is $\mathcal{F} > 0.996$, the result is presented in Fig. 2 and further discussed in Sec. II E.

We now move to the two-excitation addition problem. Here, the initial state consists of a single photon in the waveguide and the TLS excited, $|\psi(t=0)\rangle = \int_{\mathbb{R}} dx f_{\text{in}}(x) \hat{a}^\dagger(x) |0, e\rangle$. The goal is for the TLS to undergo a dynamic stimulated emission process such that the two-photon output state is a Fock state with unit probability. Solving for the two-excitation addition process in the same way as the subtraction process would relate the initial conditions to the output two-photon wavefunction, $\alpha_2(x_1, x_2, t)$. However, this is unwanted because the only constraint on the output two-photon wavefunction is for it to be separable and we do not wish to impose any further constraints such as specifying the output temporal mode.

Instead, we wish to derive the dynamic coupling for the addition process by applying reversal transformations to the subtraction process. Assuming the two-excitation subtraction process has unit probability, then the two-excitation addition process is the time-reversed process [39]. However, a time-reversal transformation is not enough to bring the Hamiltonian back into the form of Eq. (3) since the direction of travel is also flipped. Therefore, in the interaction picture, we must perform a time-reversal transformation, a translation to reposition the TLS back to the starting position, followed by a parity inversion such that the TLS still travels to the left. Moreover, the initial and final state of the subtraction process under these transformations are mapped to the final and initial state of the addition process respectively. Hence, in order to reproduce the subtraction in reverse we must prepare the initial state of the addition process according to the final state of the subtraction process. This would lead to a coupling strength that depends on the output state of the addition process, which is unwanted. To get around this issue, we make a single-mode approximation such that, the temporal mode of the single-photon wavefunction of the two-excitation subtraction process is the same as the input temporal mode, $f_{\text{in}}(-t)$, of the two-photon Fock state. This approximation is valid since their overlap is near-unity, $|\sqrt{70/69} \int_{\mathbb{R}} dx f_{\text{in}}^*(x) \lim_{t \rightarrow \infty} \beta_2(x, t)|^2 = 112/115 \approx 0.974$. All together, we perform the three transformations with the single-mode approximation and obtain the dynamic coupling strength for the two-excitation addition process that only depends on the initial state (see

Appendix B),

$$g_{\text{add},2}^*(t) = \frac{a_2 f_{\text{in}}(-t)}{\sqrt{3 \int_t^\infty dt' |f_{\text{in}}(-t')|^2}}. \quad (27)$$

Here, we have also included a variational parameter that takes the optimised value, $a_2 = 0.816$, and $f_{\text{in}}(-t)$ is the temporal mode of the initial input single-photon Fock state. The fidelity of the two-excitation addition process with the optimised dynamic coupling is $\mathcal{F} > 0.996$, the result is presented in Fig. 2 and further discussed in Sec. II E.

D. n excitations

In this subsection, we generalise our solution for two-excitation subtraction and addition processes to n -excitation processes as illustrated by the schematic of Fig. 1. The ideal n -excitation subtraction process is when the TLS absorbs a photon from an incoming n -photon Fock state with unit probability, and the outgoing state is an $(n-1)$ -photon Fock state. Conversely, the ideal n -excitation addition process is the reverse, the initially excited TLS emits a photon to an incoming $(n-1)$ -photon Fock state with unit probability and the outgoing state is a n -photon Fock state. The strategy to obtain the time-dependent coupling strength is similar to that of the two-excitation processes: we confine the dynamics to the n -excitation subspace and derive the equations of motion from the Schrödinger equation. However, solving for the unsymmetrised wavefunctions from region to region is intractable as the number of terms grow quickly. Nonetheless, making the linear approximation (the TLS only interacts with one photon in total) at appropriate steps, can greatly reduce the number of terms (see Appendix C).

We solve the n -excitation subtraction process with the an initial n -photon Fock state in the waveguide and the TLS in the ground state, i.e. $|\psi(t=0)\rangle = [\int_{\mathbb{R}} dx f_{\text{in}}(x) \hat{a}^\dagger(x)]^n |0, g\rangle / \sqrt{n!}$. The output boundary condition for n -excitation subtraction is $f_{\text{in}}(-t) = n g^*(t) e^{-G(0,t)/2} S_{1/2}(0,t)$ (see Appendix C for a derivation). Notice that, this is in the form of the general boundary condition in Eq. (24) and its solution is given by Eq. (25) with $u = n$ and $v = 1/2$. Similar to the treatment of the linearised two-excitation subtraction solution, we multiply the solution by a variational parameter, $s_n \in \mathbb{R}$, that we later optimise numerically. Explicitly, the time-dependent coupling strength for the n -excitation subtraction process is

$$g_{\text{sub},n}^*(t) = \frac{s_n f_{\text{in}}(-t)}{\sqrt{(2n-1) \int_0^t dt' |f_{\text{in}}(-t')|^2}}. \quad (28)$$

On the other hand, the initial state of the n -excitation addition process consists of an $(n-1)$ -photon Fock state

n	s_n	a_n
1	1.000	1.000
2	1.072	0.816
3	1.088	0.883
4	1.095	0.926
5	1.098	0.960

TABLE I. Numerically optimised parameters for subtraction (s_n) and addition (a_n) processes for up to five excitations.

in the waveguide with the TLS excited, i.e. $|\psi(t=0)\rangle = [\int_{\mathbb{R}} dx f_{\text{in}}(x) \hat{a}^\dagger(x)]^{n-1} |0, e\rangle / \sqrt{(n-1)!}$. Applying the time-reversal, translation and parity inversion transformations to the Hamiltonian in Eq. (3) in the same way as described in Sec. II C, we obtain the time-dependent coupling strength for the n -excitation addition process (see Appendix B). Recall that, we approximated the initial temporal mode and the output temporal mode of the subtraction processes to be the same. In fact, this approximation becomes more accurate with increasing n , as the overlap between the two increases with the excitation number (overlap ≈ 0.99). Explicitly, the coupling for addition reads

$$g_{\text{add},n}^*(t) = \frac{a_n f_{\text{in}}(-t)}{\sqrt{(2n-1) \int_t^\infty dt' |f_{\text{in}}(-t')|^2}}. \quad (29)$$

Here, $a_n \in \mathbb{R}$ is the variational parameter for the n -excitation addition process. The optimised parameters for subtraction and addition for up to five excitations are given in Table I. We emphasize that these optimised parameters also produce high fidelity for other mode shapes. Recall that the coupling strength for the single-excitation addition process is given by Eq. (10), which corresponds to setting $f_{\text{in}}(-t) \rightarrow i f_{\text{out}}(-t)$ in Eq. (29). From this perspective, the single-excitation process is unique; the initial state is fixed and the final state can be easily read off from the coupling strength.

E. Results and discussions

In this subsection, we present numerical results and discussions for subtraction and addition processes for up to five excitations. We first introduce the setup and the numerical techniques. Followed by showcasing the fidelities with and without losses. We provide an intuitive argument of how this type of dynamic coupling can arise by approximating the TLS-photon interaction by a Jaynes-Cummings model; we also point out some features that the Jaynes-Cummings model fails to predict. We show that the output temporal modes for two- and four-excitation subtraction processes are well approximated by the input temporal mode. Lastly, we present cascaded subtraction and addition with up to five TLSs.

Since the couplings considered in this work are chiral, we model the dynamics using the quantum pulses formalism in Refs. [35, 50]. Specifically, we set up an

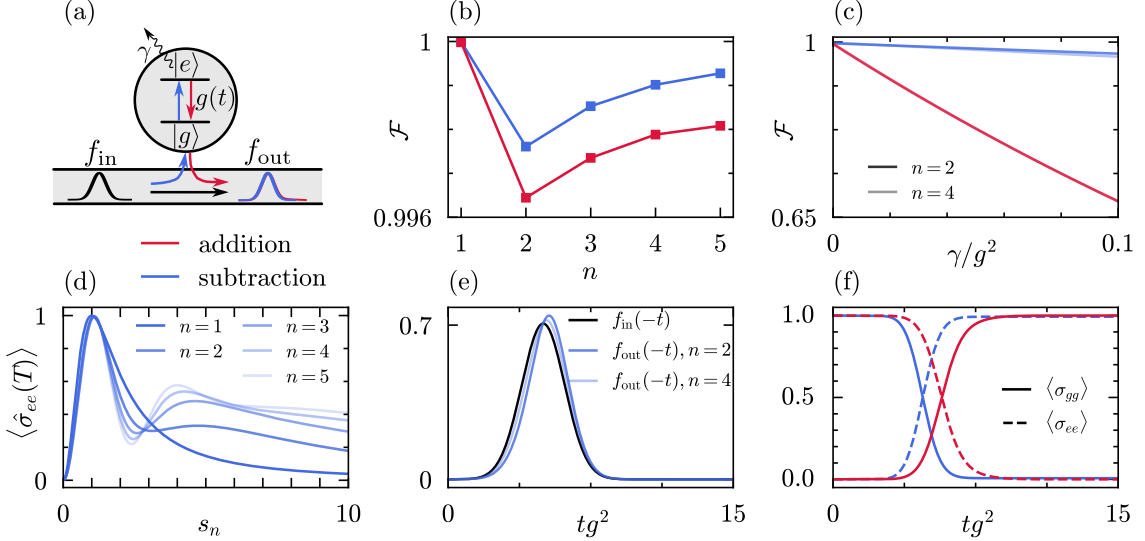


FIG. 2. Simulation results for the addition and subtraction processes, labeled by colours blue and red respectively. The schematic of both processes are depicted in (a), where f_{in} is the input temporal mode and f_{out} the output mode. The excitation in the TLS of dynamic stimulated emission follows the red arrows, the reverse process where a photon is absorbed by the TLS follows the blue arrows. Results in all sub-figures (b-f) are simulated with a Gaussian input temporal mode of width $\sigma g^2 = 2/\sqrt{\pi}$, where $g^2 = |g_{\text{sub},1}(t_0)|^2$ is the reference coupling rate of the system (see main text). (b) The lossless unconditional fidelities for the subtraction and addition processes for up to five excitations and (c) in the presence of loss for two- and four-excitation. The reduced addition fidelities in (c) are due to the TLS's idling time (see main text). (d) At final time, T , the excited state population for the subtraction process versus variational parameter s_n for up to five excitations. (e) The input Gaussian temporal mode and the output temporal modes for the two- and four-excitation subtraction processes. (f) The ground (solid) and excited (dashed) state population dynamics for the two-excitation subtraction and addition processes.

input virtual cavity in the upstream to inject the input state, followed by the TLS in the middle and a collection virtual cavity in the downstream to analyse the output state. We emphasize that these virtual cavities are absent in an experiment and they are only introduced for the numerical analysis. To analyse a multi-moded state, we factorise the first-order correlation function into a sum of orthogonal modes, $G^{(1)}(t, t') = \langle \hat{a}^\dagger(-t)\hat{a}(-t') \rangle = \sum_i \bar{n}_i f_i^*(-t)f_i(-t')$, here, $f_i(-t)$ are the orthogonal modes and \bar{n}_i are the corresponding mean photon number contained in each mode. We note that, the photon field annihilation and creation operators of $G^{(1)}(t, t')$ are evaluated just after the TLS.

To assess the performance of the dynamic stimulated emission and absorption processes, we analyse the mode with the highest mean photon number of each particular process. For the simulations without loss we solve the closed-system dynamics using a matrix-product state approach [51–53]. When considering loss, we solve an open-system Lindblad Master Equation in QuTip [54]. The schematic of the simulated addition and subtraction processes, colour-coded by red and blue respectively, are presented in Fig. 2(a). For up to five excitations, the incident states are photon Fock states in a Gaussian mode and the initial states of the TLS are prepared according to Fig. 1. We chose the input temporal mode to be a Gaussian ($f_{\text{in}}(-t) = \frac{1}{\sqrt{\sigma\sqrt{\pi}}}e^{-(t-t_0)^2/\sigma^2}$) of width

$\sigma g^2 = 2/\sqrt{\pi}$, where $g^2 = |g_{\text{sub},1}(t_0)|^2$ is a reference coupling rate that is used to define the time-scale of the dynamics and it is defined as the coupling strength of the single-photon subtraction process (Eq. (12)) evaluated at the center of a Gaussian input temporal mode. Most importantly, we chose the coupling strength for subtraction and addition for the TLS according to Eq. (28) and Eq. (29) respectively.

In analysing the performance, we define the fidelity of the n -excitation subtraction process by $\mathcal{F} = \text{Tr}[|n-1\rangle_{\text{out}}\langle n-1| \hat{\rho}]$. Here, $\hat{\rho}$ is the asymptotic final state of the TLS and the photon field; $|n-1\rangle_{\text{out}}$ is an $(n-1)$ -photon Fock state of the photon field with the corresponding temporal mode determined from factorising the first-order correlation function. We highlight that this fidelity captures both the absorption efficiency and the single-mode character of the output photon state. For the special single-excitation subtraction process, the entire output field is required to be in vacuum. Equivalently, in the lossless case, single-excitation subtraction fidelity is the excited state population at the final time i.e., $\mathcal{F} = \text{Tr}[\hat{\sigma}_{ee}\hat{\rho}]$. Similarly, the fidelity of the n -excitation addition process is $\mathcal{F} = \text{Tr}[|n\rangle_{\text{out}}\langle n| \hat{\rho}]$. In the lossless scenario, the fidelities of the subtraction (blue) and addition (red) processes are presented in Fig. 2(b). Unit fidelities are expected for the single-excitation processes as their solutions are exact; however remarkably, with slight numerical optimisation on the variational param-

eters (Tab. I), the fidelities are monotonically increasing with excitation number larger than one, from $\mathcal{F} \approx 0.998$ to $\mathcal{F} \approx 0.999$ for the subtraction processes and $\mathcal{F} \approx 0.996$ to $\mathcal{F} \approx 0.998$ for the addition processes. The slightly lower fidelities of the addition processes is likely caused by the mode mismatch before applying the reversal transformations.

The subtraction ansatz given by Eq. (28) can be intuitively understood by approximating the TLS-photon interaction as being Jaynes-Cummings-like, but with a time dependence [39]. One then approximates the photon-field operators of the interaction Hamiltonian in Eq. (3) by a product of the temporal mode and a single-mode bosonic operator i.e., $\hat{a}(-t) \rightarrow f_{\text{in}}(-t)\hat{a}$, thereby Eq. (3) becomes the Jaynes-Cummings Hamiltonian, $\hat{H}(t) = g(t)f_{\text{in}}(-t)\hat{\sigma}_+ \hat{a} + \text{h.c.}$. In this simplified model, the n -excitation subtraction process occurs when the system undergoes Rabi oscillations with the asymptotic transition, $|n, g\rangle \rightarrow |n-1, e\rangle$. A solution of the following form satisfies this transition by having the Rabi dynamics executing a π -pulse, that is $\sqrt{n} \int_0^\infty dt g(t)f_{\text{in}}(-t) = \pi/2$;

$$g^*(t) = \frac{\pi f_{\text{in}}(-t)}{4\sqrt{n \int_0^t dt' |f_{\text{in}}(-t')|^2}}. \quad (30)$$

Although the π -pulse model fails to reproduce the exact solution of the single-excitation subtraction process when $n = 1$, the only difference is a multiplicative factor. As an artifact of the Jaynes-Cummings model, the π -pulse model accounts for the variations in the Rabi frequency with the number of excitations, n . In the form of Eq. (28), the π -pulse model produces a qualitative prediction for the optimised variational parameter, $s_n^{(\pi)} = \frac{\pi}{4} \sqrt{\frac{2n-1}{n}} = \{0.785, 0.962, 1.014, 1.039, 1.054\}$ for $n = \{1, 2, \dots, 5\}$. Importantly, the π -pulse model predicts that, if the Rabi dynamics executes a π -pulse, then multiplying the coupling strength by odd integers would also satisfy the asymptotic transition of the subtraction process. This would imply that when sweeping s_n , we should observe Rabi oscillations. In Fig. 2(d), we show that this is not the case. Apart from the first peak, we do not observe unit excited state population at the final time as we sweep the variational parameter in the range, $s_n \in [0, 10]$, which highlights the limitations of the simplified Jaynes-Cummings-like model.

In Fig. 2(c), we have considered the impact of experimental imperfections on the fidelities of the two- and four-excitation processes. Here, the TLS can decay into non-guided modes and we model these loss mechanisms by including an extra Lindblad operator of the form $\hat{L}_1 = \sqrt{\gamma} \hat{\sigma}_-$ in the Lindblad Master equation. The subtraction (blue) processes are tolerant to losses with fidelities $\mathcal{F} \approx 0.97$ at 10% loss ($\gamma/g^2 = 0.1$). Because in order for the TLS to lose an excitation to the non-guided mode, it needs to absorb a photon from the guided mode, hence it is still a valid subtraction. On the other hand, the fidelities of the addition (red) processes suffer greatly

from losses, with $\mathcal{F} \approx 0.68$ at 10% loss. This is because the TLS is initial prepared in the excited state and it has to idle while waiting for the input temporal mode to arrive. During the idling time, the excitation in the TLS could spontaneous decay into non-guided modes, thereby no excitation is left to be emitted into the guided mode. To minimise the effects of losses on the addition processes in experiments, one could prepare an exponential input temporal mode and excite the TLS just as the mode is arriving such that the idling time is minimised.

Figure. 2(e) depicts the input temporal mode, $f_{\text{in}}(-t)$, and the output temporal modes, $f_{\text{out}}(-t)$, for the two- and four-excitation subtraction processes. Qualitatively, the overlap between these modes increase with the number of excitations, which justifies the approximation, $f_{\text{in}}(-t) = f_{\text{out}}(-t)$ that we have used to derive the time-dependent coupling strengths for the n -excitation addition process. In Fig. 2(f), we showcase both the ground-(solid line) and excited-state (dashed line) population dynamics for the two-excitation subtraction (blue) and addition (red) processes.

Subtracting and adding more than one single-photon can be achieved by cascading multiple TLSs. In this work, we cascade up to five TLSs and the schematics for these processes are depicted in Fig. 3(a). Ideal n -excitation cascade subtraction process occurs with the transition, $|n\rangle |g\rangle^{\otimes n} \rightarrow |0\rangle |e\rangle^{\otimes n}$, here $|n\rangle$ is an n -photon Fock state with an Gaussian input temporal mode and $|0\rangle$ is the vacuum, in other words, an n -photon Fock state excites all n TLSs. Conversely, ideal n -excitation cascaded addition process occurs when all n initially excited TLSs emit photons to produce an n -photon Fock state i.e., $|0\rangle |e\rangle^{\otimes n} \rightarrow |n\rangle |g\rangle^{\otimes n}$.

We define the fidelity of the n -excitation cascaded subtraction process to be the overlap between the output photon field and the vacuum state, in the lossless case, this is equivalent to the excited state population of all the TLSs at the final time i.e., $\mathcal{F} = \text{Tr} \left[\prod_{j=1}^n \hat{\sigma}_{ee}^j \hat{\rho} \right]$. We define the fidelity of the n -excitation cascaded addition process to be $\mathcal{F} = \text{Tr} [|n\rangle_{\text{out}} \langle n | \hat{\rho}]$. The fidelities for the cascaded subtraction and addition processes with up to five-excitations are presented in Fig. 3(b). Without conditioning on specific measurement outcomes of the TLSs, the imperfections from each individual subtraction and addition interaction (Fig. 2(b)) compound and ultimately reduce the total fidelity of the cascaded processes. For example, the fidelities are $\mathcal{F} \approx 0.97$ for both five-excitation cascade subtraction and addition processes. Moreover, Fig. 3(d-e) show that the temporal mode after interacting with each TLS is slightly delayed and changes in shape; we emphasize that the dynamic couplings for each cascaded TLS are adjusted accordingly. Although we have neglected the time taken for the photons to travel between subsequent TLSs, we do consider delays of the temporal mode due to interaction with the TLSs. Therefore extra time is needed for subsequent TLSs to reach their excited states, as shown in Fig. 3(c).

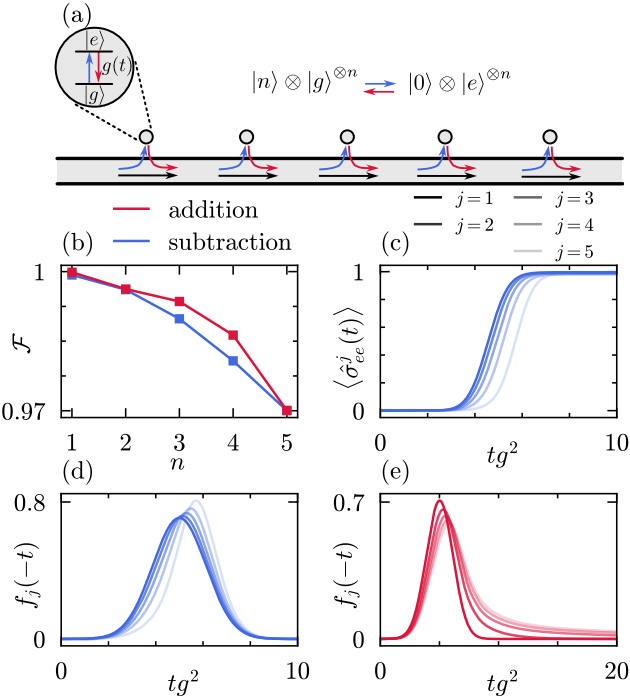


FIG. 3. Simulation results for cascading up to five TLSs each with unique dynamic couplings. The subtraction and addition processes throughout this figure are labeled by colours blue and red respectively. (a) The schematic for cascading five TLSs for dynamic stimulated emission (red arrows) and absorption (blue arrows) with the corresponding ideal transitions, $|5\rangle|g\rangle^{\otimes 5} \rightarrow |0\rangle|e\rangle^{\otimes 5}$ and $|0\rangle|e\rangle^{\otimes 5} \rightarrow |5\rangle|g\rangle^{\otimes 5}$, respectively. (b) The unconditional fidelities from single- to five-excitation cascaded addition and subtraction processes; n denotes the total number of excitations or equivalently the number of TLSs. The subtraction processes are all initialised with a Gaussian input temporal mode of width $\sigma g^2 = 2/\sqrt{\pi}$, where g^2 is a reference coupling rate (see main text). On the other hand, for the cascaded addition processes, the coupling strength of the first TLS is chosen such that it emits a photon with a Gaussian temporal mode of width $\sigma g^2 = 2/\sqrt{\pi}$. Sub-figures (c-e) show features of the five-excitation cascaded subtraction and addition. (c) The dynamics of the excited state populations for each cascaded TLS labeled by j . The temporal mode $f_j(-t)$ for subtraction (d) and addition (e) occupying the highest mean photon number before and after interacting with the j -th cascaded TLS respectively.

III. DYNAMIC STIMULATED EMISSION AND ABSORPTION USING THREE-LEVEL SYSTEMS

The processes of using TLSs to add and subtract photons introduced so far rely on modulating the coupling strength with time. This feature can be realised in circuit QED systems [55, 56] but would be infeasible to implement in optical systems. Additionally, the n -excitation addition process suffers greatly from experimental imperfections due to the idling time of the TLS as it needs to wait for the temporal mode to arrive. Hence, we are mo-

tivated to swap the TLS with a system that would be feasible to be considered in optical experiments and is more loss-tolerant.

In the spirit of Ref. [41], we introduce a Λ -type three-level system (3LS) that is driven by a coherent laser with a time-dependent Rabi frequency and phase, to effectively describe a TLS and its dynamic coupling. The milestone protocol of Ref. [41] has been experimentally demonstrated with microwave [57–59] and optical [60, 61] photons and even phonons [62]. In this section, we start with the 3LS Hamiltonian, where under large detunings, the excited state can be adiabatically eliminated leading to an effective TLS with time-dependent couplings controlled by the coherent drive. Here, we present our n -excitation subtraction and addition solutions of the required time-dependent Rabi frequency and phase of the coherent drive (see Appendix E for detail derivations of the single-, two- and n -excitation processes). Finally, we show that the performance of the 3LS is on par with that of the TLS.

A. Model

Here, we consider a Λ -type (3LS) consists of an excited state $|r\rangle$ with excitation frequency ω_0 , and two degenerate ground states $|e\rangle$ and $|g\rangle$ (see Fig. 4). On the transition from $|e\rangle$ to $|r\rangle$, the 3LS is driven by a coherent laser with frequency, ω_L , time-dependent Rabi frequency, $\Omega(t)$, and phase, $\phi(t)$. Meanwhile, the transition between $|g\rangle$ and $|r\rangle$ is coupled to the right-propagating photon field in a one-dimensional waveguide with decay rate, Γ . Under the dipole, rotating-wave and Markov approximations, the Hamiltonian to model this system reads, [41],

$$\hat{H} = \int_{\mathbb{R}} dx \hat{a}^\dagger(x)(\omega_L - i\partial_x)\hat{a}(x) + \omega_0 \hat{\sigma}_{rr} + \frac{\Omega(t)}{2} (e^{-i(\omega_L t + \phi(t))} \hat{\sigma}_{re} + \text{h.c.}) + \sqrt{\Gamma} (\hat{\sigma}_{rg} \hat{a}(0) + \text{h.c.}), \quad (31)$$

with $\hat{\sigma}_{ij} = |i\rangle\langle j|$. The first term is the free energy and the generator for propagation for the photon field. The second term is the excited state energy of the 3LS. The third and fourth terms facilitate the transition $|e\rangle \leftrightarrow |g\rangle$. We move to an interaction picture with respect to both the excited state and the photon field at the laser frequency, ω_L , and the co-moving frame of the free-propagation term in the Hamiltonian. Furthermore, under large detunings ($\Delta = \omega_L - \omega_0$), $|\Delta| \gg \Omega(t), \Gamma$, the dynamics of the excited state is suppressed, hence the excited state can be adiabatically eliminated, which produces an effective TLS with AC Stark shifts on the ground state energies that dependent on the Rabi frequency of the coherent drive and the photon field in the waveguide. Importantly, the $|e\rangle \leftrightarrow |g\rangle$ transition is now modulated by the time-dependent Rabi frequency and phase. All

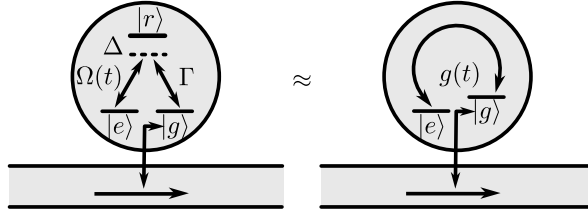


FIG. 4. Λ -type three-level system (3LS) and the effective two-level system (TLS). On the left-hand side, a full 3LS with the excited state $|r\rangle$ and degenerate ground states $|e\rangle$, $|g\rangle$; that is under a large detuned coherent drive with time-dependent Rabi frequency and phase. Adiabatically eliminating the excited state, $|r\rangle$, yields the right-hand side, an effective TLS with AC Stark shifts to the energy of the ground states.

together, the dynamics of the 3LS and the photon field can be described by an effective Hamiltonian with only the degenerate ground states, $|g\rangle$ and $|e\rangle$, and an effective time-dependent coupling strength to the photon field (see Appendix E),

$$\hat{H}_{\text{eff}} = \frac{\Gamma}{\Delta} \hat{\sigma}_{gg} \hat{a}^\dagger(-t) \hat{a}(-t) + \frac{\sqrt{\Gamma} \Omega(t)}{2\Delta} \left[e^{i\phi_g(t)} \hat{\sigma}_{eg} \hat{a}(-t) + \text{h.c.} \right]. \quad (32)$$

Note that we have eliminated the AC Stark shift of the energy of the $|e\rangle$ state by moving to an interaction picture and defining $\phi(t) = \phi_e(t) + \phi_g(t)$ and $\partial_t \phi_e(t) = -\Omega^2(t)/(4\Delta)$. The other AC Stark shift of the $|g\rangle$ state remains and it depends on the local state of the photon field. The effective time-dependent coupling is $g(t) = \sqrt{\Gamma} \Omega(t) e^{i\phi_g(t)}/(2\Delta)$ and the Rabi frequency and phase are $\Omega(t) e^{i\phi(t)}/2 = \Delta g(t) e^{-i\frac{\Delta}{\Gamma} G(0,t)}/\sqrt{\Gamma}$, where $G(0,t) = \int_0^t dt' |g(t')|^2$. We note that the Hamiltonian is very much like that of the TLS, but has included the AC Stark shift term. If we use parameters such that $\Delta \gg \Omega(t) \gg \Gamma$, then one can likely neglect the AC Stark shift term and use our TLS ansatz (Eq. (29) and Eq. (28)) to solve for the required time-dependent couplings for addition and subtraction. This approximation becomes worse for larger input photon states as $\hat{a}^\dagger(-t) \hat{a}(-t)$ increases the importance of the AC Stark shift term. Therefore, in the following sections we solve the processes with Eq. (32) in its entirety.

B. n excitations

Under the effective model of the 3LS, ideal n -excitation subtraction occurs when the 3LS is initially prepared in $|g\rangle$, an incoming n -photon Fock state generates the transition to $|e\rangle$, and the outgoing state is an $(n-1)$ -photon Fock state. In solving for the effective dynamic coupling strengths of the subtraction process, we adapt a similar treatment to the processes with a TLS but the AC Stark shift in the effective Hamiltonian in Eq. (32) brings a

level of complexity to the solutions. Nevertheless, the output boundary condition is (see Appendix E),

$$f_{\text{in}}(-t) = \frac{1 - (\xi^*/\xi)^n}{1 - \xi^*/\xi} |\xi|^2 g^*(t) e^{-\frac{\xi}{2} G(0,t)} S_{\xi/2}(0,t), \quad (33)$$

Here, $\xi = [1 + i\Gamma/(2\Delta)]^{-1}$ is a feature of the AC Stark effect. Importantly, this boundary condition is in the form of Eq. (24) and its solution is given by Eq. (25). When using 3LSs for subtractions, we modify the coupling strength with two variational parameters, for the real and imaginary parts of $u - v$ in Eq. (25). Despite including the extra parameters, the coupling strength is a solution to some boundary condition in the form of Eq. (24). Explicitly, the effective time-dependent coupling strength for the n -excitation subtraction using a 3LS is

$$g^*(t) = \frac{s_{r,n} f_{\text{in}}(-t)}{\sqrt{2 \text{Re}(\zeta) \left[\int_0^t dt' |f_{\text{in}}(-t')|^2 \right]^{1+i s_{i,n} \frac{\text{Im}(\zeta)}{\text{Re}(\zeta)}}}}, \quad (34)$$

here, $\zeta = \frac{1-(\xi^*/\xi)^n}{1-\xi^*/\xi} |\xi|^2 - \xi/2$, $\text{Im}(\cdot)$ denotes the imaginary part of a complex number and the optimised variational parameters, $s_{r,n}, s_{i,n} \in \mathbb{R}$, are given by Tab. II. Notice that, if we had neglected the AC stark shift by setting $\xi = 1$, the coupling strength reduces to the solution for the TLS in Eq. (28). Moreover, the additional variational parameter, $s_{i,n}$ would be unnecessary, since $\text{Im}(\zeta) = 0$. Nevertheless, the time-dependent Rabi frequency and phase for the n -excitation subtraction process are

$$\begin{aligned} & \frac{\Omega_{\text{sub},n}(t)}{2} e^{i\phi_{\text{sub},n}(t)} \\ &= \frac{\Delta}{\sqrt{\Gamma}} \frac{s_{r,n} f_{\text{in}}^*(-t)}{\sqrt{2 \text{Re}(\zeta) F(t)^{1+i[s_{r,n}^2 \frac{\Delta}{\Gamma} - s_{i,n} \text{Im}(\zeta)]/\text{Re}(\zeta)}}}, \end{aligned} \quad (35)$$

here, $F(t) = \int_0^t dt' |f_{\text{in}}(-t')|^2$.

Conversely, the ideal n -excitation addition process is the reverse of the subtraction process. It occurs when an incoming $(n-1)$ -photon Fock state gains a photon and leaves in an n -photon Fock state, accompanied by the $|e\rangle \rightarrow |g\rangle$ transition of the 3LS. To obtain the time-dependent Rabi frequency and phase for the addition processes, we apply the time-reversal, translation and parity inversion transformations to the subtraction process (see Appendix B). Explicitly, the time-dependent Rabi frequency and phase for the n -excitation addition process reads

$$\begin{aligned} & \frac{\Omega_{\text{add},n}(t)}{2} e^{i\phi_{\text{add},n}(t)} \\ &= \frac{\Delta}{\sqrt{\Gamma}} \frac{a_{r,n} f_{\text{in}}^*(-t)}{\sqrt{2 \text{Re}(\zeta) \tilde{F}(t)^{1-i[a_{r,n}^2 \frac{\Delta}{\Gamma} - a_{i,n} \text{Im}(\zeta)]/\text{Re}(\zeta)}}}, \end{aligned} \quad (36)$$

where $\tilde{F}(t) = \int_t^\infty dt' |f_{\text{in}}(-t')|^2$. Similarly, $a_{r,n}, a_{i,n} \in \mathbb{R}$ are the variational parameters and the optimised value

n	$s_{r,n}$	$s_{i,n}$	$a_{r,n}$	$a_{i,n}$
1	1.026	1.057	1.025	1.083
2	1.080	0.858	0.819	0.921
3	1.087	0.795	0.874	0.875
4	1.082	0.750	0.897	0.839
5	1.066	0.702	0.902	0.805

TABLE II. Numerically optimised parameters for subtraction ($s_{r,n}$, $s_{i,n}$) and addition ($a_{r,n}$, $a_{i,n}$) processes using 3LSs for up to five excitations.

are given in Tab. II. We emphasize that in the single-excitation scenario, the initial state is fixed with the 3LS in state $|e\rangle$ and the photon field in vacuum, therefore one should make the substitution $f_{\text{in}}(-t) \rightarrow i f_{\text{out}}(-t)$ in Eq. (36) such that, the final state of the photon field is a single-photon state with temporal mode $f_{\text{out}}(-t)$ (see Appendix E). Notice that from Tab. II, the variational parameters for the single-excitation processes deviate from 1, this is caused by the optimisation using the full 3LS but the solutions are derived under the effective Hamiltonian given by Eq. (32).

C. Results and discussions

In this subsection, we present and discuss the performance of the n -excitation addition and subtraction processes using 3LSs. We briefly describe the numerical setup of the full 3LS simulation. The results are presented by Fig. 5 which includes the fidelities with and without loss for up to five excitations, the time-dependent Rabi frequency and phase, the state populations and the output temporal modes for subtraction. Remarkably, both the addition and subtraction processes are tolerant to losses.

As described in Sec. II E, we use the quantum pulses formalism where single-mode states are injected and absorbed into the waveguide using virtual cavities. In this subsection, we simulated the *full* 3LS without adiabatically eliminating of the excited state. We include coupling to non-guided modes of the environment by including an additional Lindblad operator in the master equation, $\hat{L}_1 = \sqrt{\gamma} \hat{\sigma}_{gr}$.

The schematic of the n -excitation subtraction and addition processes are depicted in Fig. 5(a) by blue and red respectively. We chose the time-dependent Rabi frequency and phase for each processes according to Eq. (35) and Eq. (36). Since the analytic calculations are performed under the approximation of adiabatically eliminating the excited state, to simulate the dynamics of the full 3LS, we must be in a regime where the approximation is justified i.e., $|\Delta| \gg \Omega(t), \Gamma$. From Eq. (35) and Eq. (36), the Rabi frequency is proportional to the input temporal mode, hence choosing a wide Gaussian reduces its magnitude. In all simulations, we have set the detuning to be $\Delta/\Gamma = 5$ and the input Gaussian mode with width $\sigma\Gamma = 25$. We define the fidelities

of each processes identically to that of the TLS described in Sec. II E. The fidelity for the n -excitation subtraction process is $\mathcal{F} = \text{Tr}[|n-1\rangle_{\text{out}} \langle n-1| \hat{\rho}]$, where $|n-1\rangle_{\text{out}}$ is an $(n-1)$ -photon Fock state. On the other hand, the fidelity for the n -excitation addition process is $\mathcal{F} = \text{Tr}[|n\rangle_{\text{out}} \langle n| \hat{\rho}]$.

In Fig. 5(b), we present the fidelities of the subtraction (blue) and addition (red) processes for up to five excitations. The only approximation in the single-excitation processes is adiabatically eliminating the excited state, otherwise the expressions for the Rabi frequencies and phases are exact. Hence, both the single-excitation subtraction and addition processes have near unit fidelity with the addition process slightly higher because a single-photon state is always single-moded. For processes with excitation number greater than one, the fidelities are monotonically increasing; for subtraction the fidelity with two excitations is $\mathcal{F} \approx 0.997$ and increases to $\mathcal{F} \approx 0.999$ with five excitations, for addition, the fidelity with two excitation is $\mathcal{F} \approx 0.996$ and increases to $\mathcal{F} \approx 0.997$ with five excitations. Furthermore, the optimised parameters in Tab. II are responsible to correct for two approximations for the subtraction processes, namely, the adiabatic elimination of the excited state and the linearised analytic solutions. The addition processes have slightly lower fidelities because we have approximated the input temporal mode to be the same as the output before applying the reversal transformations to the subtraction process, Fig. 5(e) shows that this is a valid approximation. Nevertheless, this is another approximation that the optimised parameters have to correct for.

Figure 5(c) presents the fidelities of the two- and four-excitation processes with loss. The loss mechanism considered here is the 3LS decaying into non-guided modes under the $|r\rangle \rightarrow |g\rangle$ transition. Remarkably, the four-excitation subtraction process achieves $\mathcal{F} \approx 0.99$ with 10% ($\gamma/\Gamma = 0.1$) loss corresponding to a cooperativity of 10. As explained in Sec. II E, the 3LS decaying into non-guided modes is still a valid subtraction on the guided mode. Most importantly, the addition processes are also tolerant to losses, unlike the TLS where the excited state can spontaneously decays into non-guided modes whilst idling before the input temporal mode arrives. Here, the 3LS only gets excited by the Rabi drive as the temporal mode arrives, hence greatly reducing the impact of the spontaneous decay on the fidelities.

We show that the adiabatic condition, $|\Delta| \gg \Omega(t)$ is satisfied by plotting the time-dependent Rabi frequency and phase for the two-excitation subtraction (blue) and addition (red) processes in Fig. 5(d). In Fig. 5(e), we show that the input temporal mode is approximately equal to the output temporal mode for the two- and four-excitation subtraction processes, thus it is appropriate to equate them for the reversal transformations. Figure 5(f) shows that the 3LS indeed acts like a TLS with most of the state population shared between the two ground states while the $|r\rangle$ state is remains largely unpopulated.

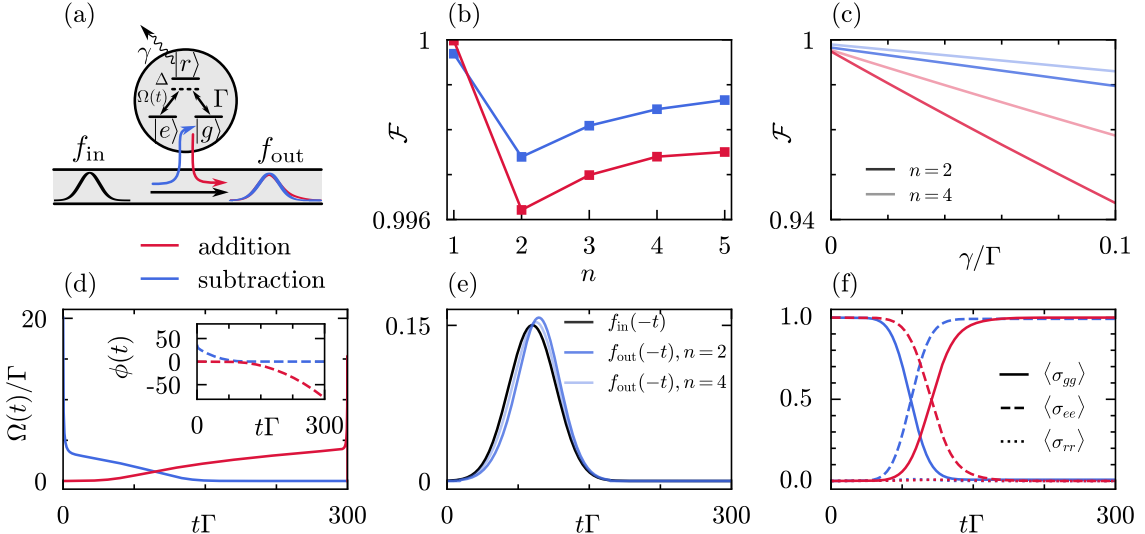


FIG. 5. Simulation results with the full 3LS. The subtraction and addition processes throughout this figure are labeled by colours blue and red respectively. (a) The schematic of the 3LS dynamic stimulated emission (red arrows) and absorption (blue arrows) with input and output temporal modes labeled by f_{in} and f_{out} respectively. Results in all sub-figures are simulated with detuning $\Delta/\Gamma = 5$ and with a Gaussian input temporal mode of width $\sigma\Gamma = 25$. The lossless unconditional fidelities for the subtraction and addition processes for up to five excitations are presented in (b) and with loss for two- and four-excitation in (c). In (d), the time-dependent Rabi frequency (solid) and phase (inset, dashed) for the two-excitation subtraction and addition processes. (e) The input Gaussian temporal mode (black) and the output temporal modes for the two- and four-excitation subtraction processes. (f) The ground states, $|g\rangle$ (solid), $|e\rangle$ (dashed) and the excited state (dotted) population dynamics for the two-excitation subtraction and addition processes.

IV. GENERATION OF NON-GAUSSIAN SUPERPOSITION STATES

In previous sections, we used TLSs that are dynamically coupled to the propagating photon field to prepare photon Fock states with high fidelities. While photon Fock states have a wide range of applications in photonic quantum technologies [63, 64], non-Gaussian superpositions of Fock states such as the Schrödinger cat states and GKP states have enjoyed unparalleled attention in encoding quantum information [3, 11–13]. Typical state preparation protocols rely on conditional measurements on the outputs of a linear optical networks, which have low success probabilities. In this section, we explore the possibilities of using dynamic stimulated emission and absorption to prepare these non-Gaussian superposition states. However, since our solutions are strictly excitation-number dependent, having a TLS interact with a superposition state would likely render the process with a degree of nondeterminism. Therefore, we must herald on successful subtraction or addition of photons by measuring the TLS after the interaction. First, we demonstrate that, successive subtraction *or* addition of photons with a squeezed vacuum input state can prepare cat states with high fidelity. Next, we show that dynamic stimulated emission can be used to add a photon to an incoming general Gaussian state with high fidelity and success probability.

A. Cat states

Here, we prepare cat states using successive subtractions. Cat states are defined as a superposition of opposite phase coherent states, $|\text{cat}_{\alpha,\pm}\rangle \propto |\alpha\rangle \pm |-\alpha\rangle$. Large-scale cat states are key resources in quantum technologies. However, the efficient preparation of optical cat states have remained a challenge. Conventionally, optical cat states are prepared by the successive action of photon subtractions on a squeezed vacuum [17, 18, 21]. In linear optical protocols, photon subtractions are typically realised by inserting beam splitters and looking for photon-number-resolving detection patterns. Recently, Lund *et al.* [39] showed that optical cat states can be prepared with higher success probabilities using a TLS with multiplexing. In this work, we show that cat states can be prepared via dynamic absorption. In Fig. 6(a), we cascade up to five TLSs to herald five subtractions (blue) from a 10 dB squeezed vacuum input. The Wigner functions after each subtraction are highlighted by blue boxes. Since our solutions for high-fidelity n -excitation subtraction, given by Eq. (28), varies depending on the number of excitations, the process of dynamic absorption is not expected to be deterministic when the input is a superposition state. Moreover, it is unclear which dynamic coupling would produce an optimal result. Inspired by Ref. [39], we require that the dynamic absorption process acts similarly to the annihilation operator on the photon field i.e., we wish to execute the transition

$|g\rangle|\alpha\rangle \rightarrow |e\rangle|\alpha\rangle$, where $|\alpha\rangle$ is a coherent state. But this transition violates the conservation of the total excitation therefore, the transition can only be satisfied by a nondeterministic process. Here, we emphasize that there is a trade off between the fidelity and success probability; in the extreme case, a trivial process where no photon is absorbed would produce unit fidelity but also zero success probability. We found that by using the dynamic coupling $g(t) = 0.15g_{\text{sub},1}(t)$, the transition with $\alpha = \sqrt{10}$ can be approximately satisfied with fidelity $\mathcal{F} \approx 0.997$ and success probability approximately equal to 0.635. Recall that $g_{\text{sub},1}(t)$ is the single-excitation subtraction solution, given by Eq. (12). Therefore, we have chosen to use this dynamic coupling for each of the cascaded TLS depicted in Fig. 6(a). We note that the slightly changing mode shape after each interaction is accounted for in the dynamic couplings. The final state should ideally be a single-mode state of the photon field after other system and bath are traced out. The fidelity, success probability and the cat state size after each subtraction are presented by blues boxes in Fig. 6(b-d).

Preparing large-scale cat states using successive subtractions is ultimately not efficient, Fig. 6(c) shows that at five subtractions, the cumulative success probability is approximately 1%; this high degree of nondeterminism can be reasoned back to having a squeezed-vacuum input state. Using non-Gaussian input states, characterised by their non-zero stellar rank, can greatly improve the success probabilities of preparing large-scale cat states [52, 63, 64]. However, efficiently preparing optical non-Gaussian input states itself is also a challenge.

Here, we instead prepare cat states by successive *additions* of photons with a 10 dB squeezed vacuum input, see Fig. 6(a) for a schematic. Throughout this work, we have relied on the deterministic feature of the subtraction processes on Fock states such that under reversal transformations we obtain the dynamic couplings which facilitate deterministic addition processes. However, as Fig. 6 suggests, and mentioned in Sec. II C, the subtraction processes with a superposition input state are not deterministic. There are two factors that contribute to the nondeterminism, namely; the input squeezed vacuum state has a significant population of vacuum which cannot excite the TLS, and the nonlinear response of the TLS produce distinct interactions between different Fock states mean that a superposition cannot excite a TLS deterministically. If we had used a dynamic coupling obtained from the reversal transformations of the nondeterministic subtraction process for the addition process, the output state would be multi-moded. Hence, to produce a single-mode output state, we must introduce a time-dependent coupling strength for the addition of photons on superposition states. The following expression is our ansatz and it is motivated by solving the Schrödinger equation for the addition process on an n -excitation Fock

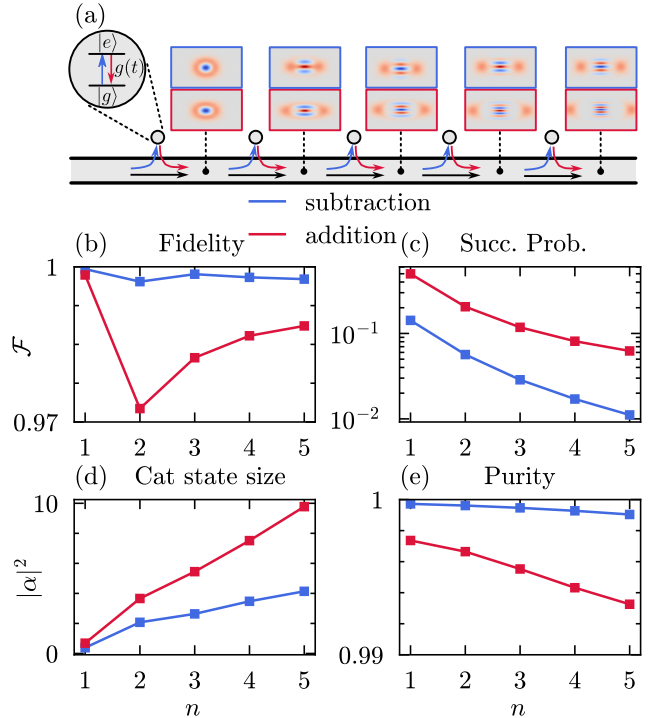


FIG. 6. Simulation results of cat state generation using successive dynamic stimulated emissions or absorptions. The emission and absorption processes throughout this figure are labeled by colours red and blue respectively. In (a), the schematic for successive subtractions or additions of single-photons by cascading five TLSs (grey circles) with a 10 dB squeezed vacuum input state. Here, successive subtractions and additions are distinct processes and the Wigner functions are presented in the highlight boxes with single-mode state after each interaction is the optimally unsqueezed. In the colourmap of the Wigner functions, red (blue) indicates positive (negative) values. In sub-figures (b-c), the horizontal axis labels the number of successive subtractions or additions, from one up to five. In (b) the fidelity after each interaction, the fidelity is calculated against a cat state after the output state is optimally unsqueezed. In (c), the success probability after n interactions. (d) The output cat state size, $|\alpha|^2$. (e) The purity and it reflects if the output state is single-moded.

state (see Appendix D);

$$g_{\text{add}}^*(t) = \frac{q_1 f_{\text{in}}(-t)}{\sqrt{1 - q_2 \int_0^t dt' |f_{\text{in}}(-t')|^2}}. \quad (37)$$

Here, $f_{\text{in}}(-t)$ is the temporal mode just before the photon field interacts with the TLS, and $q_1, q_2 \in \mathbb{R}$ are variational parameters with $q_2 \leq 1$. This ansatz offers great flexibility and notice that, for $q_2 = 1$ and $q_1 = a_n/\sqrt{2n-1}$, we recover the n -excitation addition coupling strength given by Eq. (29). We cascade up to five TLSs with time-dependent coupling strength according to Eq. (37). We optimised the parameters for the first TLS for success probability without sacrificing too much purity (or preserving a single-mode); the values of the

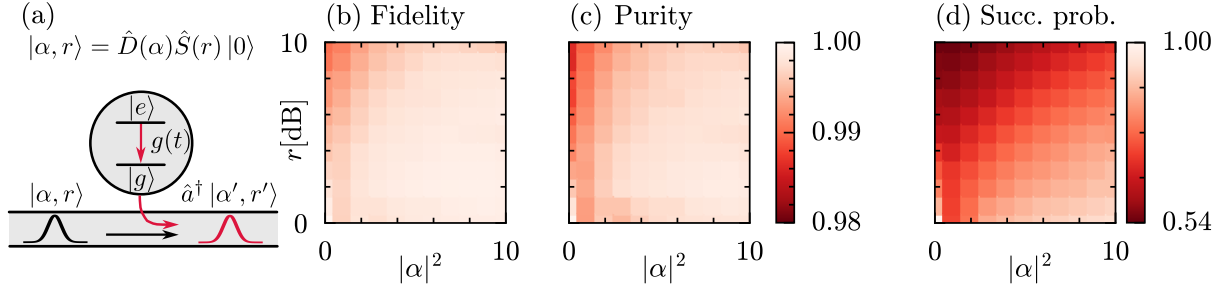


FIG. 7. Preparation of photon-added Gaussian states. In (a), the schematic where we use dynamic stimulated emission of the TLS to add a photon to a displaced squeezed vacuum state with displacement, α and squeezing strength, r . The target state is the normalised state after applying the creation operator on a different displaced squeezed vacuum. We considered displacement in the range $\alpha \in [0, \sqrt{10}]$ and squeezing up to 10 dB. In (b-d), the fidelities, purities and the success probabilities for a combination of displacements and squeezing strengths.

optimised parameters are $\{q_1, q_2\} = \{0.509, 0.425\}$. Notice that a creation operator or an annihilation operator acting on a squeezed vacuum produces the same state; hence, in Fig. 6(b) we observe overlapping fidelities for a single-photon subtracted or added squeezed vacuum state. However, successive action of the creation operator on a squeezed vacuum state produces a different state from that of the annihilation operator. Therefore, without compromising on the fidelities we found that the variational parameters, $\{q_1, q_2\} = \{1/\sqrt{10}, 1/10\}$ for the subsequent TLSs, are a middle ground for generating large-scale cat states with increasing fidelities and high success probabilities. Although Fig. 6(b) shows that the cat states generated after each round of addition have lower fidelities than that with the subtractions, the successive addition protocol is however far more efficient, at nearly an order-of-magnitude higher in success probability (Fig. 6(c)) and the size of the generated cat state (Fig. 6(d)) is much larger. The higher success probabilities come at a cost of lowered purities i.e., the state of the photon field is less contained in a single-mode, but nonetheless the purities are above 0.99 after five successive additions of single-photons (Fig. 6(e)).

B. Photon-added Gaussian state

A general Gaussian pure state can be described as a displaced and squeezed vacuum, $\hat{D}(\alpha)\hat{S}(r)|0\rangle$; here, $\hat{D}(\alpha) = e^{\alpha\hat{a}^\dagger - \alpha^*\hat{a}}$ and $\hat{S}(r) = e^{-\frac{r}{2}(\hat{a}^2 - \hat{a}^{\dagger 2})}$ are the single-mode displacement operator and squeezing operator, respectively. In this subsection, we consider $\{\alpha, r\} \in \mathbb{R}$. We refer to a photon-added Gaussian state as the normalised state after applying a photon creation operator on a displaced squeezed vacuum. In this subsection, we use dynamic stimulated emission of a TLS to produce a photon-added Gaussian state. These states are key resource states as they serve as starting points for generating non-Gaussian states of higher stellar ranks [65].

Figure 7(a) shows a schematic of dynamic stimulated

emission of a photon to a displaced squeezed vacuum in a temporal mode. The target state is a photon-added displaced squeezed vacuum. Note that the output state does not necessarily have the same displacement and squeezing values. This means that for a Gaussian state, the TLS mimics the action of the creation operator up to a Gaussian operation. In the absence of loss, dynamic stimulated emission preserves excitation number. The differences in displacement and squeezing between the initial state and the target state can be qualitatively explained by the difference between an excitation-conserving unitary evolution and the action of the creation operator. Suppose the process shown in Fig. 7(a) is deterministic, by the excitation-conserving Hamiltonian in Eq. (3), the excitation number of the photon field after the TLS has emitted a photon is $\sinh^2(r) + |\alpha|^2 + 1$; to match the excitation number, the displacement and squeezing on the target state must be different except for the case with vacuum. For conditional processes, the excitation number is not conserved; hence we allow the target state to have different amounts of displacement and squeezing.

In this subsection, we used the ansatz given by Eq. (37) for the addition of a single-photon with the two variational parameters, $\{q_1, q_2\}$. Since a particular dynamic coupling cannot deterministically carry out single-photon addition for a superposition of Fock states, we must condition on measuring the TLS in the ground state to herald a successful addition. We optimised the variational parameters for a balance between success probability and purity for the input displacements in the range, $\alpha \in [0, \sqrt{10}]$ and squeezing strength from 0 dB to 10 dB.

The fidelities against photon-added Gaussian states and the purities are present in Fig. 7(b-c); the success probabilities of addition are presented in Fig. 7(d). The fidelities, purities and success probabilities decrease from unity with increased values of squeezing on the vacuum; at 10 dB of squeezing the fidelity and the success probability reduce to approximately 0.98 and 0.55 respectively. The reductions in the fidelity and success probability for the photon-added squeezed vacuum can be explained by the increased variance in the Fock-state distribution with

increased values of squeezing on the vacuum. Nonetheless, this feature can be compensated by introducing displacements, since it can reduce the relative difference in the excitation number of the dominant probability amplitudes. Moreover, the photon-added coherent state with $|\alpha|^2 = 10$, can achieve approximately 0.999 fidelity and 0.94 success probability, as shown in Fig. 7. On average, most photon-added Gaussian states have fidelities above 0.99 and success probabilities above 0.6. We note that the TLS can introduce anti-displacement and anti-squeezing, the discrepancies between the initial and the target displacements and squeezing strengths are presented by Fig. 8 in Appendix. D.

V. CONCLUSIONS AND OUTLOOK

In summary, we have introduced the concept of dynamic stimulated emission and absorption of two-level systems by providing the time-dependent coupling strengths to the n -excitation addition and subtraction processes; we showed that our solutions can achieve fidelities greater than 0.996 for arbitrary number of excitations. We cascade up to five TLSs for five successive additions or subtractions of single photons and the unconditional fidelities are above 0.97, demonstrating the possibility of preparing n -excitation Fock states using quantum emitters. Furthermore, we showed that the same n -excitation addition and subtraction processes can occur if the TLS and its time-dependent coupling strength are replaced with a 3LS that is driven by a coherent laser with a time-dependent Rabi frequency and phase, which can be realised in optical experiments. As a proof-of-concept, we demonstrated high success probabilities of preparing Schrödinger cat states from a squeezed vacuum input by cascading up to five TLSs for single-photon subtractions and additions. However, a more practical use of quantum emitters may be preparing photon-added Gaussian states. While Gaussian states such as the squeezed vacuum state has been widely considered as resource states for the preparation of useful non-Gaussian states [17, 19–

23], the lack of non-Gaussianity reflected by their zero stellar rank and the lack of mean photon number, ultimately hinder the efficiency of preparing exotic non-Gaussian states such as the large-scale cat states or the GKP states. On the other hand, using a photon-added Gaussian state with stellar rank one [65] or other few-photon non-Gaussian states can greatly improve the feasibility of preparing exotic non-Gaussian states using linear optical protocols [52, 64, 66].

Future directions include improvement on the success probabilities of single-photon subtraction and addition when the input is a superposition state, thus directly improving the efficiency of preparing a photon-added Gaussian state. Moreover, one could cascade quantum emitters and prepare multi-photon-added Gaussian states, which have higher stellar ranks and could potentially improve the preparation of exotic non-Gaussian states. On the other hand, by entangling the cascaded quantum emitters, one can also prepare superposition states in a temporal mode. The cubic phase state is another key non-Gaussian state for universal bosonic quantum computation [67–70], incorporating quantum emitters into the preparation schemes could potentially improve the efficiency. Ultimately, our work provides a path for integrating quantum emitters into optical non-Gaussian state preparation.

ACKNOWLEDGMENTS

H.L. thanks Yangming Wang for useful discussions and acknowledges support from the Sydney Quantum Academy. S.M. acknowledges support from the Australian Research Council (ARC) via the Future Fellowship, ‘Emergent many-body phenomena in engineered quantum optical systems’, project no. FT200100844. M.M. acknowledges support from the Office of Naval Research (Award No. N00014-24-1-2052). P.S.S. gratefully acknowledges support from the S2I-Gupta Fellowship. F.Y. gratefully acknowledges support from the NSF Graduate Research Fellowship.

[1] S. D. Bartlett, B. C. Sanders, S. L. Braunstein, and K. Nemoto, Efficient classical simulation of continuous variable quantum information processes, *Phys. Rev. Lett.* **88**, 097904 (2002).

[2] A. Mari and J. Eisert, Positive wigner functions render classical simulation of quantum computation efficient, *Phys. Rev. Lett.* **109**, 230503 (2012).

[3] T. C. Ralph, A. Gilchrist, G. J. Milburn, W. J. Munro, and S. Glancy, Quantum computation with optical coherent states, *Phys. Rev. A* **68**, 042319 (2003).

[4] M. Mirrahimi, Z. Leghtas, V. V. Albert, S. Touzard, R. J. Schoelkopf, L. Jiang, and M. H. Devoret, Dynamically protected cat-qubits: a new paradigm for universal quantum computation, *New Journal of Physics* **16**, 045014 (2014).

[5] E. Knill, R. Laflamme, and G. J. Milburn, A scheme for efficient quantum computation with linear optics, *Nature* **409**, 46 (2001).

[6] P. Kok, W. J. Munro, K. Nemoto, T. C. Ralph, J. P. Dowling, and G. J. Milburn, Linear optical quantum computing with photonic qubits, *Rev. Mod. Phys.* **79**, 135 (2007).

[7] W. J. Munro, K. Nemoto, G. J. Milburn, and S. L. Braunstein, Weak-force detection with superposed coherent states, *Phys. Rev. A* **66**, 023819 (2002).

[8] A. Gilchrist, K. Nemoto, W. J. Munro, T. C. Ralph, S. Glancy, S. L. Braunstein, and G. J. Milburn, Schrödinger cats and their power for quantum informa-

tion processing, *Journal of Optics B: Quantum and Semiclassical Optics* **6**, S828 (2004).

[9] S. L. Braunstein and P. van Loock, Quantum information with continuous variables, *Rev. Mod. Phys.* **77**, 513 (2005).

[10] J. B. Brask, I. Rigas, E. S. Polzik, U. L. Andersen, and A. S. Sørensen, Hybrid long-distance entanglement distribution protocol, *Phys. Rev. Lett.* **105**, 160501 (2010).

[11] A. L. Grimsmo, J. Combes, and B. Q. Baragiola, Quantum computing with rotation-symmetric bosonic codes, *Phys. Rev. X* **10**, 011058 (2020).

[12] D. Gottesman, A. Kitaev, and J. Preskill, Encoding a qubit in an oscillator, *Phys. Rev. A* **64**, 012310 (2001).

[13] A. L. Grimsmo and S. Puri, Quantum error correction with the gottesman-kitaev-preskill code, *PRX Quantum* **2**, 020101 (2021).

[14] N. Ofek, A. Petrenko, R. Heeres, P. Reinhold, Z. Leghtas, B. Vlastakis, Y. Liu, L. Frunzio, S. M. Girvin, L. Jiang, M. Mirrahimi, M. H. Devoret, and R. J. Schoelkopf, Extending the lifetime of a quantum bit with error correction in superconducting circuits, *Nature* **536**, 441 (2016).

[15] C. Flühmann, T. L. Nguyen, M. Marinelli, V. Negnevitsky, K. Mehta, and J. P. Home, Encoding a qubit in a trapped-ion mechanical oscillator, *Nature* **566**, 513 (2019).

[16] V. G. Matsos, C. H. Valahu, T. Navickas, A. D. Rao, M. J. Millican, X. C. Kolesnikow, M. J. Biercuk, and T. R. Tan, Robust and deterministic preparation of bosonic logical states in a trapped ion, *Phys. Rev. Lett.* **133**, 050602 (2024).

[17] M. Dakna, T. Anhut, T. Opatrný, L. Knöll, and D.-G. Welsch, Generating schrödinger-cat-like states by means of conditional measurements on a beam splitter, *Phys. Rev. A* **55**, 3184 (1997).

[18] A. Ourjoumtsev, R. Tualle-Brouri, J. Laurat, and P. Grangier, Generating optical schrödinger kittens for quantum information processing, *Science* **312**, 83 (2006), <https://www.science.org/doi/pdf/10.1126/science.1122858>.

[19] A. Ourjoumtsev, A. Dantan, R. Tualle-Brouri, and P. Grangier, Increasing entanglement between gaussian states by coherent photon subtraction, *Phys. Rev. Lett.* **98**, 030502 (2007).

[20] M. V. Larsen, J. E. Bourassa, S. Kocsis, J. F. Tasker, R. S. Chadwick, C. González-Arciniegas, J. Hastrup, C. E. Lopetegui-González, F. M. Miatto, A. Motamedi, R. Noro, G. Roeland, R. Baby, H. Chen, P. Contu, I. Di Luch, C. Drago, M. Giesbrecht, T. Grainge, I. Krasnokutska, M. Menotti, B. Morrison, C. Puviraj, K. Rezaei Shad, B. Hussain, J. McMahon, J. E. Ortmann, M. J. Collins, C. Ma, D. S. Phillips, M. Seymour, Q. Y. Tang, B. Yang, Z. Vernon, R. N. Alexander, and D. H. Mahler, Integrated photonic source of gottesman-kitaev-preskill qubits, *Nature* **642**, 587 (2025).

[21] K. Takase, J.-i. Yoshikawa, W. Asavanant, M. Endo, and A. Furusawa, Generation of optical schrödinger cat states by generalized photon subtraction, *Phys. Rev. A* **103**, 013710 (2021).

[22] K. Takase, F. Hanamura, H. Nagayoshi, J. E. Bourassa, R. N. Alexander, A. Kawasaki, W. Asavanant, M. Endo, and A. Furusawa, Generation of flying logical qubits using generalized photon subtraction with adaptive gaussian operations, *Phys. Rev. A* **110**, 012436 (2024).

[23] F. Hanamura, K. Takase, H. Nagayoshi, R. Ide, W. Asavanant, K. Fukui, P. Marek, R. Filip, and A. Furusawa, Beyond stellar rank: Control parameters for scalable optical non-gaussian state generation (2025), arXiv:2509.06255 [quant-ph].

[24] N. Tomm, A. Javadi, N. O. Antoniadis, D. Najer, M. C. Löbl, A. R. Korsch, R. Schott, S. R. Valentin, A. D. Wieck, A. Ludwig, and R. J. Warburton, A bright and fast source of coherent single photons, *Nature Nanotechnology* **16**, 399 (2021).

[25] P. Lodahl, S. Mahmoodian, and S. Stobbe, Interfacing single photons and single quantum dots with photonic nanostructures, *Rev. Mod. Phys.* **87**, 347 (2015).

[26] I. Aharonovich, D. Englund, and M. Toth, Solid-state single-photon emitters, *Nature Photonics* **10**, 631 (2016).

[27] P. Senellart, G. Solomon, and A. White, High-performance semiconductor quantum-dot single-photon sources, *Nature Nanotechnology* **12**, 1026 (2017).

[28] P. Thomas, L. Ruscio, O. Morin, and G. Rempe, Efficient generation of entangled multiphoton graph states from a single atom, *Nature* **608**, 677 (2022).

[29] X. Ding, Y.-P. Guo, M.-C. Xu, R.-Z. Liu, G.-Y. Zou, J.-Y. Zhao, Z.-X. Ge, Q.-H. Zhang, H.-L. Liu, L.-J. Wang, M.-C. Chen, H. Wang, Y.-M. He, Y.-H. Huo, C.-Y. Lu, and J.-W. Pan, High-efficiency single-photon source above the loss-tolerant threshold for efficient linear optical quantum computing, *Nature Photonics* **19**, 387 (2025).

[30] R. H. Dicke, Coherence in spontaneous radiation processes, *Phys. Rev.* **93**, 99 (1954).

[31] V. I. Yudson, Dynamics of integrable quantum systems, *Sov. Phys. JETP* **88**, 1043 (1985).

[32] V. Paulisch, M. Perarnau-Llobet, A. González-Tudela, and J. I. Cirac, Quantum metrology with one-dimensional superradiant photonic states, *Phys. Rev. A* **99**, 043807 (2019).

[33] D. Valente, Y. Li, J. P. Poizat, J. M. Gérard, L. C. Kwek, M. F. Santos, and A. Auffèves, Optimal irreversible stimulated emission, *New Journal of Physics* **14**, 083029 (2012).

[34] K. A. Fischer, Exact calculation of stimulated emission driven by pulsed light, *OSA Continuum* **1**, 772 (2018).

[35] A. H. Kiilerich and K. Mølmer, Input-output theory with quantum pulses, *Phys. Rev. Lett.* **123**, 123604 (2019).

[36] S. Mahmoodian, G. Calajó, D. E. Chang, K. Hammerer, and A. S. Sørensen, Dynamics of many-body photon bound states in chiral waveguide qed, *Phys. Rev. X* **10**, 031011 (2020).

[37] T. C. Ralph, I. Söllner, S. Mahmoodian, A. G. White, and P. Lodahl, Photon sorting, efficient bell measurements, and a deterministic controlled- z gate using a passive two-level nonlinearity, *Phys. Rev. Lett.* **114**, 173603 (2015).

[38] F. Yang, M. M. Lund, T. Pohl, P. Lodahl, and K. Mølmer, Deterministic photon sorting in waveguide qed systems, *Phys. Rev. Lett.* **128**, 213603 (2022).

[39] M. M. Lund, F. Yang, V. R. Christiansen, D. Kornovan, and K. Mølmer, Subtraction and addition of propagating photons by two-level emitters, *Phys. Rev. Lett.* **133**, 103601 (2024).

[40] L. Serino, J. Gil-Lopez, M. Stefszky, R. Ricken, C. Eigner, B. Brecht, and C. Silberhorn, Realization of a multi-output quantum pulse gate for decoding high-dimensional temporal modes of single-photon states, *PRX Quantum* **4**, 020306 (2023).

[41] J. I. Cirac, P. Zoller, H. J. Kimble, and H. Mabuchi, Quantum state transfer and entanglement distribution among distant nodes in a quantum network, *Phys. Rev. Lett.* **78**, 3221 (1997).

[42] K. M. Gheri, K. Ellinger, T. Pellizzari, and P. Zoller, Photon-wavepackets as flying quantum bits, *Fortschritte der Physik* **46**, 401 (1998).

[43] J. E. Gough and G. Zhang, Generating nonclassical quantum input field states with modulating filters, *EPJ Quantum Technology* **2**, 15 (2015).

[44] H. I. Nurdin, M. R. James, and N. Yamamoto, Perfect single device absorber of arbitrary traveling single photon fields with a tunable coupling parameter: A qsde approach, in *2016 IEEE 55th Conference on Decision and Control (CDC)* (2016) pp. 2513–2518.

[45] P. Lodahl, S. Mahmoodian, S. Stobbe, A. Rauschenbeutel, P. Schneeweiss, J. Volz, H. Pichler, and P. Zoller, Chiral quantum optics, *Nature* **541**, 473 (2017).

[46] I. Söllner, S. Mahmoodian, S. L. Hansen, L. Midolo, A. Javadi, G. Kiršanskė, T. Perngolato, H. El-Ella, E. H. Lee, J. D. Song, S. Stobbe, and P. Lodahl, Deterministic photon–emitter coupling in chiral photonic circuits, *Nature Nanotechnology* **10**, 775 (2015).

[47] D. Suárez-Forero, M. Jalali Mehrabad, C. Vega, A. González-Tudela, and M. Hafezi, Chiral quantum optics: Recent developments and future directions, *PRX Quantum* **6**, 020101 (2025).

[48] C. Joshi, F. Yang, and M. Mirhosseini, Resonance fluorescence of a chiral artificial atom, *Phys. Rev. X* **13**, 021039 (2023).

[49] J.-T. Shen and S. Fan, Strongly correlated multiparticle transport in one dimension through a quantum impurity, *Phys. Rev. A* **76**, 062709 (2007).

[50] J. Combes, J. Kerckhoff, and M. Sarovar, The slh framework for modeling quantum input-output networks, *Advances in Physics: X* **2**, 784 (2017), <https://doi.org/10.1080/23746149.2017.1343097>.

[51] H. Pichler and P. Zoller, Photonic circuits with time delays and quantum feedback, *Phys. Rev. Lett.* **116**, 093601 (2016).

[52] H. Luo and S. Mahmoodian, Efficient optical cat state generation using squeezed few-photon superposition states (2024), arXiv:2412.14798 [quant-ph].

[53] M. Fishman, S. R. White, and E. M. Stoudenmire, The ITensor Software Library for Tensor Network Calculations, *SciPost Phys. Codebases* , 4 (2022).

[54] N. Lambert, E. Gigu‘ere, P. Menczel, B. Li, P. Hopf, G. Su‘arez, M. Gali, J. Lishman, R. Gadhvi, R. Agarwal, A. Galicia, N. Shammah, P. Nation, J. R. Johansson, S. Ahmed, S. Cross, A. Pitchford, and F. Nori, Qutip 5: The quantum toolbox in Python, *Physics Reports* **1153**, 1 (2026).

[55] A. N. Korotkov, Flying microwave qubits with nearly perfect transfer efficiency, *Phys. Rev. B* **84**, 014510 (2011).

[56] Y. Yin, Y. Chen, D. Sank, P. J. J. O’Malley, T. C. White, R. Barends, J. Kelly, E. Lucero, M. Mariantoni, A. Megrant, C. Neill, A. Vainsencher, J. Wenner, A. N. Korotkov, A. N. Cleland, and J. M. Martinis, Catch and release of microwave photon states, *Phys. Rev. Lett.* **110**, 107001 (2013).

[57] M. Pechal, L. Huthmacher, C. Eichler, S. Zeytinoğlu, A. A. Abdumalikov, S. Berger, A. Wallraff, and S. Filipp, Microwave-controlled generation of shaped single photons in circuit quantum electrodynamics, *Phys. Rev. X* **4**, 041010 (2014).

[58] P. Kurpiers, P. Magnard, T. Walter, B. Royer, M. Pechal, J. Heinsoo, Y. Salathé, A. Akin, S. Storz, J. C. Besse, S. Gasparinetti, A. Blais, and A. Wallraff, Deterministic quantum state transfer and remote entanglement using microwave photons, *Nature* **558**, 264 (2018).

[59] C. J. Axline, L. D. Burkhardt, W. Pfaff, M. Zhang, K. Chou, P. Campagne-Ibarcq, P. Reinhold, L. Frunzio, S. M. Girvin, L. Jiang, M. H. Devoret, and R. J. Schoelkopf, On-demand quantum state transfer and entanglement between remote microwave cavity memories, *Nature Physics* **14**, 705 (2018).

[60] C.-W. Chou, J. Laurat, H. Deng, K. S. Choi, H. de Riedmatten, D. Felinto, and H. J. Kimble, Functional quantum nodes for entanglement distribution over scalable quantum networks, *Science* **316**, 1316 (2007), <https://www.science.org/doi/pdf/10.1126/science.1140300>.

[61] S. Ritter, C. Nölleke, C. Hahn, A. Reiserer, A. Neuzner, M. Uphoff, M. Mücke, E. Figueroa, J. Bochmann, and G. Rempe, An elementary quantum network of single atoms in optical cavities, *Nature* **484**, 195 (2012).

[62] A. Bienfait, K. J. Satzinger, Y. P. Zhong, H.-S. Chang, M.-H. Chou, C. R. Conner, É. Dumur, J. Grebel, G. A. Peairs, R. G. Povey, and A. N. Cleland, Phonon-mediated quantum state transfer and remote qubit entanglement, *Science* **364**, 368 (2019).

[63] A. Ourjoumtsev, H. Jeong, R. Tualle-Brouri, and P. Grangier, Generation of optical ‘schrödinger cats’ from photon number states, *Nature* **448**, 784 (2007).

[64] M. S. Winnel, J. J. Guanzon, D. Singh, and T. C. Ralph, Deterministic preparation of optical squeezed cat and gottesman-kitaev-preskill states, *Phys. Rev. Lett.* **132**, 230602 (2024).

[65] U. Chabaud, D. Markham, and F. Grosshans, Stellar representation of non-gaussian quantum states, *Phys. Rev. Lett.* **124**, 063605 (2020).

[66] J. Hastrup, J. S. Neergaard-Nielsen, and U. L. Andersen, Deterministic generation of a four-component optical cat state, *Opt. Lett.* **45**, 640 (2020).

[67] S. Lloyd and S. L. Braunstein, Quantum computation over continuous variables, *Phys. Rev. Lett.* **82**, 1784 (1999).

[68] M. Gu, C. Weedbrook, N. C. Menicucci, T. C. Ralph, and P. van Loock, Quantum computing with continuous-variable clusters, *Phys. Rev. A* **79**, 062318 (2009).

[69] K. Miyata, H. Ogawa, P. Marek, R. Filip, H. Yonezawa, J.-i. Yoshikawa, and A. Furusawa, Implementation of a quantum cubic gate by an adaptive non-gaussian measurement, *Phys. Rev. A* **93**, 022301 (2016).

[70] M. Yukawa, K. Miyata, T. Mizuta, H. Yonezawa, P. Marek, R. Filip, and A. Furusawa, Generating superposition of up-to three photons for continuous variable quantum information processing, *Opt. Express* **21**, 5529 (2013).

Appendix A: The general boundary condition and its solution

In this Appendix, we derive the solution of the general boundary condition presented in Eq. (24) in the main text. In the following, we find an explicit expression of $g(t)$ from the equation

$$f(-t) = ug^*(t) \int_0^t dt' g(t') e^{vG(t,t')} f(-t'), \quad (\text{A1})$$

where $u, v \in \mathbb{C}$ and $f(-t)$ is a square-integrable function and $G(0, t) = \int_0^t dt' |g(t')|^2$. We start with an ansatz of the form,

$$g^*(t) = \frac{f(-t)}{aF(t)^b}, \quad (\text{A2})$$

where $F(t) = \int_0^t dt' |f(-t')|^2$, $a \in \mathbb{R}$ and $b \in \mathbb{C}$ with $\text{Re}(b) = 1/2$. Substituting the ansatz into Eq. (A1), we have

$$1 = \frac{u}{a^2} F(t)^{-\frac{v}{a^2}-b} \int_0^t dt' F(t')^{\frac{v}{a^2}-b^*} \partial_{t'} F(t'). \quad (\text{A3})$$

Performing the integral with $F(0) = 0$ we have,

$$1 = \frac{u}{a^2} \frac{F(t)^{-\frac{v}{a^2}-b}}{\frac{v}{a^2}-b^*+1} F(t)^{\frac{v}{a^2}-b^*+1}. \quad (\text{A4})$$

To satisfy the above equation, we arrive at two constraints on the parameters in our ansatz,

$$v + a^2(1 - b^*) = u, \quad (\text{A5})$$

$$b + b^* = 1. \quad (\text{A6})$$

The second constraint is automatically satisfied by setting $\text{Re}(b) = 1/2$. Separating the first constraint into its real and imaginary part, we can solve for a by taking the real part. Then substituting a^2 into the imaginary part of the constraint allows us to solve for $\text{Im}(b)$. Together, the solution for a and b are

$$a = \sqrt{2 \text{Re}(u - v)}, \quad (\text{A7})$$

$$b = \frac{1}{2} + i \frac{\text{Im}(u) - \text{Im}(v)}{2 \text{Re}(u - v)} = \frac{u - v}{2 \text{Re}(u - v)}. \quad (\text{A8})$$

Then we have the explicit expression for $g(t)$, and it is presented in the main text as Eq. (25)

$$g^*(t) = \frac{f(-t)}{\sqrt{2 \text{Re}(u - v) F(t)^{\frac{u-v}{\text{Re}(u-v)}}}}. \quad (\text{A9})$$

Notice that $\text{Re}(u - v) \neq 0$ in the above expression.

Appendix B: Time and space reversal

Here we present the derivation of the dynamic coupling for the single-photon addition process using a TLS and a 3LS. This Appendix is relevant for obtaining Eq. (27), Eq. (29) and Eq. (36) from Eq. (26), Eq. (28) and Eq. (35) respectively.

Photon subtraction via TLS processes are near deterministic, hence the reversed process is the photon addition process. Suppose the Hamiltonian that performs the photon subtraction process is $H_s(t) = g_s(t)\hat{\sigma}_+ \hat{a}(-t) + g_s^*(t)\hat{a}^\dagger(-t)\hat{\sigma}_-$. To find the Hamiltonian, $H_a(t) = g_a(t)\hat{\sigma}_+ \hat{a}(-t) + g_a^*(t)\hat{a}^\dagger(-t)\hat{\sigma}_-$, that performs the photon addition process, we need to apply the time-reversal $\hat{\Theta}$, translation $\hat{T}(r)$, and parity-reversal \hat{P} transformations to the subtraction Hamiltonian, $H_s(t)$. In this appendix, the subscripts of relevant quantities label the corresponding processes. The intuitive explanation behind each transformation is that: the time-reversal generates the reverse process, but in the interaction picture, the TLS has traveled to position $x = -t_f$, therefore we must return it to the origin by translation, lastly, the parity un-flips the direction of travel caused by the time-reversal transformation.

Let us introduce the operators by defining their actions on the photon field annihilation operator,

$$\hat{\Theta}\hat{a}(x)\hat{\Theta}^{-1} = \hat{a}(x), \quad \hat{\Theta}i\hat{\Theta}^{-1} = -i, \quad (B1)$$

$$\hat{T}(r)\hat{a}(x)\hat{T}^{-1}(r) = \hat{a}(x+r), \quad (B2)$$

$$\hat{\mathcal{P}}\hat{a}(x)\hat{\mathcal{P}}^{-1} = \hat{a}(-x). \quad (B3)$$

These operators act trivially on the TLS operators. Given that for ideal photon subtraction we have $|\psi_s(t_f)\rangle = \hat{U}_s(t_f, 0)|\psi_s(0)\rangle$, applying the three transformations we have

$$\hat{U}_a(t_f, 0) = \hat{\mathcal{P}}\hat{T}(t_f)\hat{\Theta}\hat{U}_s^\dagger(t_f, 0)(\hat{\mathcal{P}}\hat{T}(t_f)\hat{\Theta})^{-1} = \mathcal{T} \exp\left\{-i\int_0^{t_f} dt \ (g_s^*(t_f-t)\hat{\sigma}_+\hat{a}(-t) + g_s(t_f-t)\hat{a}^\dagger(-t)\hat{\sigma}_-)\right\}, \quad (B4)$$

where $\mathcal{T} \exp\{\}$ denotes the time-ordered exponential. We define the initial and final states of the addition by

$$|\psi_a(0)\rangle = \hat{\mathcal{P}}\hat{T}(t_f)\hat{\Theta}|\psi_s(t_f)\rangle, \quad |\psi_a(t_f)\rangle = \hat{\mathcal{P}}\hat{T}(t_f)\hat{\Theta}|\psi_s(0)\rangle. \quad (B5)$$

Then we have $|\psi_a(t_f)\rangle = \hat{U}_a(t_f, 0)|\psi_a(0)\rangle$ with

$$g_a(t) = g_s^*(t_f - t). \quad (B6)$$

Taking the infinite-time limit ($t_f \rightarrow \infty$) produces Eq. (26) and Eq. (28) of the main text. Recall that $g_s(t)$ depends on the input temporal mode of the initial state, $|\psi_s(0)\rangle$. Under these transformations, the final state of the subtraction process is mapped to the initial state of the addition process and vice versa. The dynamic coupling strength $g_a(t)$ would have to depend on the final state of the addition process, which is unwanted. Ideally the dynamic coupling should only depend on the initial state. Hence, to use the dynamic coupling in the ways described in the main text, we must make another approximation such that the initial and final states of the process share the same temporal mode (see Sec. II C and Sec. II E of the main text for justifications of making this approximation).

The full 3LS is described by a different Hamiltonian (see Eq. (31)), but the key time dependences that facilitate both the dynamic stimulated emission and absorption processes are the dynamic Rabi frequencies and phases. Applying the same argument as above, we obtain the Rabi frequency and phase for the single-photon addition process from the subtraction process, i.e. Eq. (36) from Eq. (35) of the main text. Explicitly, the relation is

$$\frac{\Omega_a(t)}{2}e^{i\phi_a(t)} = \frac{\Omega_s(t_f-t)}{2}e^{-i\phi_s(t_f-t)}. \quad (B7)$$

Appendix C: Linearised n -excitation subtraction

In this Appendix, we derive the ansatz of time-dependent coupling for the n -excitation subtraction process. The strategy is split the unsymmetrised wavefunction in different regions and solve the Schrödinger equation sequentially from region to region. To keep track of the rapidly growing number of terms, we introduce the linear approximation at appropriate steps. Finally, we arrive at a general boundary that has the form of Eq. (24) of the main text and the explicit expression for the time-dependent coupling strength is given by Eq. (25) and derived in Appendix A.

Initialising with an n -excitation Fock state, and by the conservation of excitation, the ansatz of the n -excitation subspace that captures all of the dynamics is

$$|\psi(t)\rangle = \frac{1}{\sqrt{n!}} \int_{\mathbb{R}^n} d^n \mathbf{x} \ \alpha(\mathbf{x}, t) \hat{\mathbf{a}}^\dagger(\mathbf{x}) |0, g\rangle + \frac{1}{\sqrt{(n-1)!}} \int_{\mathbb{R}^{n-1}} d^{n-1} \mathbf{x} \ \beta(\mathbf{x}, t) \hat{\mathbf{a}}^\dagger(\mathbf{x}) |0, e\rangle, \quad (C1)$$

where $d^j \mathbf{x} = dx_1 dx_2 \dots dx_j$, $\hat{\mathbf{a}}^\dagger(\mathbf{x}) = \hat{a}^\dagger(x_1) \hat{a}^\dagger(x_2) \dots \hat{a}^\dagger(x_j)$ and j is the dimension of \mathbf{x} . In the n -excitation subspace, $\alpha(\mathbf{x}, t)$ is the symmetric wavefunction corresponds to n -photon with the TLS in the ground state. Similarly, $\beta(\mathbf{x}, t)$ is the symmetric wavefunction corresponds to $(n-1)$ -photon with an excited TLS. Moreover, $\alpha(\mathbf{x}, t)$ and $\beta(\mathbf{x}, t)$ are understood to have n and $n-1$ position arguments respectively. From the Schrödinger equation, the equations of motion relate the wavefunctions by,

$$i\partial_t \alpha(\mathbf{x}, t) = \frac{g^*(t)}{\sqrt{n}} \sum_{j=1}^n \beta(\mathbf{x}, t) \delta(x_j + t), \quad (C2)$$

$$i\partial_t \beta(\mathbf{x}, t) = \sqrt{n} g(t) \alpha(\mathbf{x}, t) |_{x_m = -t}. \quad (C3)$$

Abusing the notation, the position argument, \mathbf{x} , of the n -photon wavefunction has n dimensions, while the position argument of the $(n-1)$ -photon wavefunction on the right-hand side of Eq. (C2) has $n-1$ dimensions, the missing position variable, x_j , appears in the δ -function and each term in the sum exhausts all n position variables, such that the right-hand side is also symmetric; e.g. see Eq. (14) for the two-excitation case. Likewise in Eq. (C3), the missing position variable of the $(n-1)$ -photon wavefunction is the one evaluated at $x_m = -t$ on the right-hand side, e.g. Eq. (15). Restricting to $x_1 \geq x_2 \geq \dots \geq x_n$, we work with the unsymmetrised n -photon and $(n-1)$ -photon wavefunctions; we label them in regions with respect to the position orderings of the TLS and the photons in a manner similar to the two-excitation scenario of Sec. II C. For example, $\alpha_m(\mathbf{x}, t)$ is the n -photon wavefunction in the region $x_1 \geq \dots \geq x_m \geq -t \geq x_{m+1} \geq \dots \geq x_n$, again, the subscript denotes the number of photons to the right of the TLS, in this case, m photons. Similarly, $\beta_m(\mathbf{x}, t)$ is the $(n-1)$ -photon wavefunction in the region $x_1 \geq \dots \geq x_{m-1} \geq -t \geq x_{m+1} \geq \dots \geq x_n$ with the subscript denoting the m -th photon is absorbed; additionally, it signals the position variable, x_m , is missing from the position argument, \mathbf{x} , i.e. $\beta_m(\mathbf{x}, t) = \beta_m(x_1, \dots, x_{m-1}, x_{m+1}, \dots, x_n, t)$.

Integrating Eq. (C2) away from the position of the photons, produces the free propagation condition and integrating over the position of each of the photons reveal the effects of the interactions in the form of n boundary conditions; particularly, the boundary condition that is a consequence of the interaction between the TLS and the m -th photon is

$$\alpha_m(\mathbf{x}, t) \Big|_{x_m=-t} - \alpha_{m-1}(\mathbf{x}, t) \Big|_{x_m=-t} = -i \frac{g^*(t)}{\sqrt{n}} \beta_m(\mathbf{x}, t), \quad (\text{C4})$$

with $m = 1, 2, \dots, n$. Together with the regularisation condition—when any one of the photons is evaluated at the position of the TLS, the unsymmetrical n -photon wavefunction is the average of the wavefunction in neighbouring regions, i.e. $\alpha_{\text{unsym}}(\mathbf{x}, t)|_{x_m=-t} = [\alpha_{m-1}(\mathbf{x}, t)|_{x_m=-t} + \alpha_m(\mathbf{x}, t)|_{x_m=-t}]/2$ —and the above boundary condition, Eq. (C3) produces n differential equations,

$$\partial_t \beta_m(\mathbf{x}, t) = -|g(t)|^2 \beta_m(\mathbf{x}, t)/2 - i\sqrt{n}g(t)\alpha_{m-1}(\mathbf{x}, t) \Big|_{x_m=-t} \quad (\text{C5})$$

where the corresponding domain are $t \in [-x_{m-1}, -x_m]$ with $x_0 = 0$.

We now solve the n -excitation subtraction process with the an initial n -photon Fock state in the waveguide and the TLS in the ground state,

$$|\psi(t=0)\rangle = \frac{1}{\sqrt{n!}} \left[\int_{\mathbb{R}} dx f_{\text{in}}(x) \hat{a}^\dagger(x) \right]^n |0, g\rangle. \quad (\text{C6})$$

By the free propagation property, the n -photon unsymmetrised wavefunction before any interactions is $\alpha_0(\mathbf{x}, t) = \alpha_0(\mathbf{x}, 0) = \prod_{j=1}^n f_{\text{in}}(x_j)$. The solution given by Eq. (C5) for $\beta_1(\mathbf{x}, t)$ is

$$\beta_1(\mathbf{x}, t) = -i\sqrt{n} \prod_{j=2}^n f_{\text{in}}(x_j) e^{-G(0,t)/2} S_{1/2}(0, t), \quad (\text{C7})$$

recall that $S_v(a, b) = \int_a^b dt' g(t') e^{vG(a, t')} f_{\text{in}}(-t')$ from Eq. (11). From the boundary condition in Eq. (C4), we can relate n -photon unsymmetrised wavefunction in the following region, $\alpha_1(\mathbf{x}, t)$, to the initial conditions by

$$\alpha_1(\mathbf{x}, t) \Big|_{x_1=-t} = \prod_{j=2}^n f_{\text{in}}(x_j) \left[f_{\text{in}}(-t) - g^*(t) e^{-G(0,t)/2} S_{1/2}(0, t) \right]. \quad (\text{C8})$$

Instead of solving for $\beta_2(\mathbf{x}, t)$ and $\alpha_2(\mathbf{x}, t)$, we introduce the linear approximation step by step, $x_2 = -t$, such that the TLS does not interact with subsequent photons. In other words, $\beta_2(\mathbf{x}, t)$ and $\alpha_2(\mathbf{x}, t)$ only have contributions from free propagation.

The same argument can be applied to both unsymmetriesd wavefunctions in any region, provided we introduce the linear approximation appropriately, i.e. we can relate the $(n-1)$ -photon wavefunctions in arbitrary regions to the first region, i.e. $\beta_m(\mathbf{x}, t)|_{x_{1:m-1}=-t} = \beta_1(\mathbf{x}, t)|_{x_{2:m}=-t}$ with $x_{1:m} = -t$ denoting $x_j = -t$ for $j = 1, 2, \dots, m$. This is because Eq. (C3) does not contain any δ -functions, hence the relation is simply a result of matching the wavefunctions at the boundary of each region. To see the matching boundary condition in general, let us introduce the position argument, \mathbf{y} , with $n-1$ dimensions, for the $(n-1)$ -photon wavefunction. We label the unsymmetrical $(n-1)$ -photon wavefunction by $\beta_m(\mathbf{y}, t)$ if it is in the region with position ordering $y_1 \geq \dots \geq y_{m-1} \geq -t \geq y_m \geq \dots \geq y_{n-1}$. Then

integrating Eq. (C3) with a vanishing interval centered at $t = -y_{m-1}$ produces the matching boundary condition that relates the wavefunction in neighbouring regions, $\beta_m(\mathbf{y}, -y_{m-1}) = \beta_{m-1}(\mathbf{y}, -y_{m-1})$, which is the same as

$$\beta_m(\mathbf{y}, t) \Big|_{y_{m-1} = -t} = \beta_{m-1}(\mathbf{y}, t) \Big|_{y_{m-1} = -t}, \quad (\text{C9})$$

up to a change of variable. Reiterating this expression until the label of the right-hand side reaches 1, we relate the wavefunction with label m to label 1,

$$\beta_m(\mathbf{y}, t) \Big|_{y_{1:m-1} = -t} = \beta_1(\mathbf{y}, t) \Big|_{y_{1:m-1} = -t}. \quad (\text{C10})$$

Relating the position argument, \mathbf{y} , to the position argument of the n -photon wavefunction, \mathbf{x} , we must pay carefully attention to the meaning of each label. Specifically, $\beta_m(\mathbf{x}, t)$ is the wavefunction corresponding to the m -th photon absorbed and hence it is understood that x_m should be missing from its position argument. Therefore, on the left-hand side, we evaluate $y_{1:m-1} = x_{1:m-1} = -t$ and $y_{m:n-1} = x_{m+1:n}$. Likewise, on the right-hand side, we evaluate $y_{1:m-1} = x_{2:m} = -t$ and $y_{m:n-1} = x_{m+1:n}$. All together we have the matching boundary condition that relates the $(n-1)$ -photon wavefunction in region labeled by m to 1, using the position arguments of the n -photon wavefunction,

$$\beta_m(\mathbf{x}, t) \Big|_{x_{1:m-1} = -t} = \beta_1(\mathbf{x}, t) \Big|_{x_{2:m} = -t}. \quad (\text{C11})$$

Combining this result with the boundary condition in Eq. (C4) we have the linearised boundary condition relating the n -photon wavefunctions in neighbouring regions to the initial conditions,

$$\alpha_m(\mathbf{x}, t) \Big|_{x_{1:m} = -t} - \alpha_{m-1}(\mathbf{x}, t) \Big|_{x_{1:m} = -t} = -i \frac{g^*(t)}{\sqrt{n}} \beta_m(\mathbf{x}, t) \Big|_{x_{1:m-1} = -t} = -i \frac{g^*(t)}{\sqrt{n}} \beta_1(\mathbf{x}, t) \Big|_{x_{2:m} = -t}. \quad (\text{C12})$$

By induction, the closed form of the n -photon wavefunction with label m in terms of the initial conditions with the appropriate linearisations is

$$\alpha_m(\mathbf{x}, t) \Big|_{x_{1:m} = -t} = \prod_{j=m+1}^n f_{\text{in}}(x_j) f_{\text{in}}^{m-1}(-t) \left[f_{\text{in}}(-t) - mg^*(t) e^{-G(0,t)/2} S_{1/2}(0, t) \right]. \quad (\text{C13})$$

We prove the above closed form by induction. Since $\alpha_0(\mathbf{x}, t)$ and $\alpha_1(\mathbf{x}, t)|_{x_1 = -t}$ are already in the closed form. From the linearised boundary condition in Eq. (C12) and applying the induction step we have,

$$\begin{aligned} \alpha_{m+1}(\mathbf{x}, t) \Big|_{x_{1:m+1} = -t} &= \alpha_m(\mathbf{x}, t) \Big|_{x_{1:m+1} = -t} - i \frac{g^*(t)}{\sqrt{n}} \beta_1(\mathbf{x}, t) \Big|_{x_{2:m+1} = -t} \\ &= \prod_{j=m+2}^n f_{\text{in}}(x_j) f_{\text{in}}^m(-t) \left[f_{\text{in}}(-t) - mg^*(t) e^{-G(0,t)/2} S_{1/2}(0, t) \right] \end{aligned} \quad (\text{C14})$$

$$- \prod_{j=m+2}^n f_{\text{in}}(x_j) f_{\text{in}}^m(-t) g^*(t) e^{-G(0,t)/2} S_{1/2}(0, t) \quad (\text{C15})$$

$$= \prod_{j=m+2}^n f_{\text{in}}(x_j) f_{\text{in}}^m(-t) \left[f_{\text{in}}(-t) - (m+1)g^*(t) e^{-G(0,t)/2} S_{1/2}(0, t) \right], \quad (\text{C16})$$

as required.

Lastly, the necessary output boundary condition for the ideal n -excitation subtraction process is $\alpha_n(\mathbf{x}, t) = 0$; together with the linear approximation, Eq. (C4) becomes the linearised output boundary condition,

$$\sqrt{n} \alpha_{n-1}(\mathbf{x}, t) \Big|_{x_{1:n} = -t} = ig^*(t) \beta_n(\mathbf{x}, t) \Big|_{x_{1:n-1} = -t} = ig^*(t) \beta_1(\mathbf{x}, t) \Big|_{x_{2:n} = -t}. \quad (\text{C17})$$

We emphasize that the solution obtained from the above boundary condition will not guarantee the ideal n -excitation subtraction process but it provides a high-performance ansatz. In terms of the initial conditions, the linearised output boundary condition, and according to Appendix A, the time-dependent coupling strength are

$$f_{\text{in}}(-t) = ng^*(t) e^{-G(0,t)/2} S_{1/2}(0, t), \quad g^*(t) = \frac{f_{\text{in}}(-t)}{\sqrt{(2n-1) \int_0^t dt' |f_{\text{in}}(-t')|^2}}. \quad (\text{C18})$$

Appendix D: Photon addition ansatz for superposition states

Here we provide a motivation for the ansatz given by Eq. (37) which facilitates the single-photon addition process when the input is a superposition state. We also present the differences in displacements and squeezing strengths between the prepared state and an ideal photon-added Gaussian state.

As mentioned in the main text, since the subtraction process with an superposition is nondeterministic, then using the reversed dynamic coupling for the addition process would lead to a multi-mode output state. Therefore, we must choose an alternate coupling strength. In this Appendix, we solve the Schrödinger equation for the n -excitation single-photon addition process directly. In order to obtain an explicit expression for the dynamic coupling, we still need to make the linear approximation described in Appendix C. The procedure is largely the same as Appendix C, except for the initial state has changed to an $(n-1)$ -photon Fock state with an excited TLS,

$$|\psi(t=0)\rangle = \frac{1}{\sqrt{(n-1)!}} \left[\int_{\mathbb{R}} dx f_{\text{in}}(x) \hat{a}^\dagger(x) \right]^{n-1} |0, e\rangle. \quad (\text{D1})$$

The corresponding unsymmetrised wavefunctions before any interactions are $\alpha_0(\mathbf{x}, t) = 0$ and $\beta_1(\mathbf{x}, 0) = \prod_{j=2}^n f_{\text{in}}(x_j)$. Solving Eq. (C5) for $\beta_1(\mathbf{x}, t)$, we obtain

$$\beta_1(\mathbf{x}, t) = e^{-G(0,t)/2} \prod_{j=2}^n f_{\text{in}}(x_j). \quad (\text{D2})$$

From Eq. (C4), the unsymmetrised n -photon wavefunction in the region with label 1 reads

$$\alpha_1(\mathbf{x}, t)|_{x_1=-t} = -i \frac{g^*(t)}{\sqrt{n}} e^{-G(0,t)/2} \prod_{j=2}^n f_{\text{in}}(x_j). \quad (\text{D3})$$

This corresponds to the TLS emitting a photon before any photons from the $(n-1)$ -photon Fock state has arrived. Akin to Appendix C, we introduce the linear approximation in steps. The closed form of the unsymmetrised n -photon wavefunction in the region with label m is

$$\alpha_m(\mathbf{x}, t) \Big|_{x_{1:m}=-t} = -im \frac{g^*(t)}{\sqrt{n}} e^{-G(0,t)/2} f_{\text{in}}^{m-1}(-t) \prod_{j=m+1}^n f_{\text{in}}(x_j). \quad (\text{D4})$$

We prove the above closed form by induction. Since $\alpha_0(\mathbf{x}, t)$ and $\alpha_1(\mathbf{x}, t)$ are already in the closed form, we apply the induction step with Eq. (C12);

$$\alpha_{m+1}(\mathbf{x}, t) \Big|_{x_{1:m+1}=-t} = \alpha_m(\mathbf{x}, t) \Big|_{x_{1:m+1}=-t} - i \frac{g^*(t)}{\sqrt{n}} \beta_1(\mathbf{x}, t) \Big|_{x_{2:m+1}=-t} \quad (\text{D5})$$

$$\begin{aligned} &= -im \frac{g^*(t)}{\sqrt{n}} e^{-G(0,t)/2} f_{\text{in}}^m(-t) \prod_{j=m+2}^n f_{\text{in}}(x_j) - i \frac{g^*(t)}{\sqrt{n}} e^{-G(0,t)/2} f_{\text{in}}^m(-t) \prod_{j=m+2}^n f_{\text{in}}(x_j) \\ &= -i(m+1) \frac{g^*(t)}{\sqrt{n}} e^{-G(0,t)/2} f_{\text{in}}^m(-t) \prod_{j=m+2}^n f_{\text{in}}(x_j), \end{aligned} \quad (\text{D6})$$

as required.

We require the output n -photon wavefunction to be a Fock state, i.e. the unsymmetrised wavefunction in the region n must be $\alpha_n(\mathbf{x}, t) = \prod_{j=1}^n f_{\text{out}}(x_j)$, where $f_{\text{out}}(x)$ is a normalised mode function. Using the closed form of the unsymmetrised n -photon wavefunction we can relate the desired output wavefunction to the initial condition,

$$f_{\text{out}}^n(-t) = -i\sqrt{n} g^*(-t) e^{-G(-0,t)/2} f_{\text{in}}^{n-1}(-t). \quad (\text{D7})$$

The explicit expression for the dynamic coupling can be obtained by taking the squared modulus and integrating $|f_{\text{out}}^n(-t)/f_{\text{in}}^{n-1}(-t)|^2 = -n\partial_t e^{-G(0,t)}$ from 0 to t . Finally,

$$g^*(t) = \frac{if_{\text{out}}^n(-t)}{f_{\text{in}}^{n-1}(-t) \sqrt{n - \int_0^t dt' |f_{\text{out}}^n(-t')/f_{\text{in}}^{n-1}(-t')|^2}}. \quad (\text{D8})$$

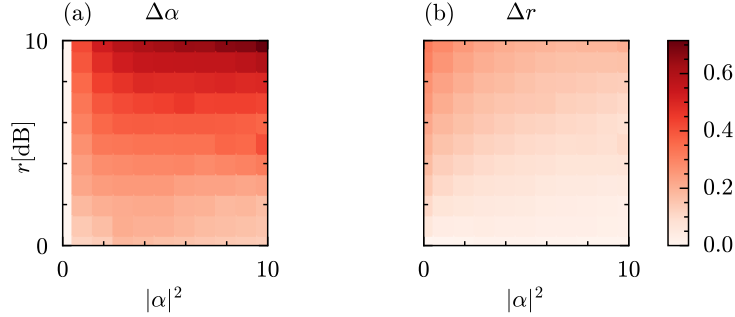


FIG. 8. Differences in displacement (a) and squeezing (b) between the prepared state and the ideal photon-added Gaussian state. The differences are defined as $\Delta\alpha = \alpha - \alpha'$ in (a) and $\Delta r = r - r'$ in (b). Here α is the displacement parameter on the input Gaussian state and α' is that of the target photon-added Gaussian state, and similarly for the squeezings r and r' .

Notice that in the single-excitation case ($n = 1$), the expression is identical to Eq. (10). However, this ansatz would not produce the desired addition processes when the excitation number is greater than one. From here we make modifications to this coupling strength to improve its flexibility. First, we approximate the output mode with the input mode $f_{\text{out}}(-t) = f_{\text{in}}(-t)$ such that it only depends on the initial conditions. Notice that when the input state is a Fock state, we are allowed to omit the global phase of the mode function, whereas for a superposition input state, we must set the global phase to 1 such that we do not introduce any unwanted relative phases within the superposition of Fock states. Furthermore, we include additional variational parameters, $\{q_1, q_2\} \in \mathbb{R}$, such that our ansatz reads

$$g^*(t) = \frac{q_1 f_{\text{in}}(-t)}{\sqrt{1 - q_2 \int_0^t dt' |f_{\text{in}}(-t')|^2}}, \quad (\text{D9})$$

where $q_2 \leq 1$. The above ansatz offers a wide range of flexibility; specifically, q_1 controls the overall magnitude, while q_2 can dramatically change the time-dependence of the ansatz. By choosing $\{q_1, q_2\} = \{1/\sqrt{n}, 1/n\}$, we recover Eq. (D8). Moreover, if $q_2 = 0$, the coupling is proportional to the mode function; and if we set $\{q_1, q_2\} = \{a_n/\sqrt{2n-1}, 1\}$, we would recover the coupling for the n -excitation addition process given by Eq. (29).

As mentioned in Sec. IV A, we use Eq. (D9) as the dynamic coupling for a TLS to add a photon to a displaced squeezed vacuum state, $|\alpha, r\rangle$. We optimised the variational parameters in Eq. (D9) such that the process has high probability of success without compromising on the fidelity against a target photon-added displaced squeezed vacuum, $|\alpha', r'\rangle$. In this process, a TLS can introduce additional displacement and squeezings, therefore we allow different displacements and squeezings between the target state and the output state, the differences are presented in Fig. 8. We found that the anti-displacement becomes significant when the input Gaussian state is highly squeezed. Conversely, the anti-squeezing is only noticeable when the initial Gaussian state is not displaced.

Appendix E: Three-level system

In this appendix, we provide details of how we derive the time-dependent coupling for the three-level system (3LS) presented in Sec. III of the main text. We derive the result [41], that an effective TLS with a time-dependent coupling is obtained using a Λ -type 3LS with a time-dependent drive. By adiabatically eliminating the excited state, we arrive at an effective Hamiltonian with time-dependent couplings between the ground states and the waveguide. We present this derivation to introduce the system using our notation, which then allows us to move on to our new result of solving for the time-dependence required for dynamic stimulated emission.

We start with a Λ -type 3LS with an excited state $|r\rangle$ and two degenerate ground states $|e\rangle$ and $|g\rangle$. The 3LS has excitation frequency ω_0 and the $|e\rangle$ to $|r\rangle$ transition is driven by a laser with frequency ω_L , time-dependent Rabi frequency $\Omega(t)$, and phase $\phi(t)$. The transition between $|g\rangle$ and $|r\rangle$ is coupled to the waveguide with decay rate Γ . The waveguide is modeled by a right-propagating photon field whose dispersion is linearised about the frequency ω_L . The Hamiltonian for this system is

$$\hat{H} = \int dx \hat{a}^\dagger(x)(\omega_L - i\partial_x)\hat{a}(x) + \omega_0\hat{\sigma}_{rr} + \frac{\Omega(t)}{2} \left[e^{-i(\omega_L t + \phi(t))} \hat{\sigma}_{re} + \text{h.c.} \right] + \sqrt{\Gamma} [\hat{\sigma}_{rg}\hat{a}(0) + \text{h.c.}], \quad (\text{E1})$$

where $\hat{\sigma}_{ij} = |i\rangle\langle j|$ and $\hat{a}(x)$ is the photon field annihilation operator at position x . Moving to an interaction picture with respect to the excited state and the photon field at the laser frequency ω_L , the Hamiltonian is

$$\hat{H} = -\Delta\hat{\sigma}_{rr} + \frac{\Omega(t)}{2} \left[e^{-i\phi(t)}\hat{\sigma}_{re} + \text{h.c.} \right] + \sqrt{\Gamma} [\hat{\sigma}_{rg}\hat{a}(-t) + \text{h.c.}], \quad (\text{E2})$$

where $\Delta = \omega_L - \omega_0$.

1. Adiabatic elimination

Here we adiabatically eliminate the excited state, $|r\rangle$ and show that the 3LS can be effectively described by a TLS. From the Heisenberg picture, the equation of motion for transition operators are

$$i\partial_t\hat{\sigma}_{re} = \Delta\hat{\sigma}_{re} - \sqrt{\Gamma}\hat{a}^\dagger(-t)\hat{\sigma}_{ge} + \frac{\Omega(t)}{2}e^{i\phi(t)}(\hat{\sigma}_{rr} - \hat{\sigma}_{ee}), \quad (\text{E3})$$

$$i\partial_t\hat{\sigma}_{rg} = \Delta\hat{\sigma}_{rg} + \sqrt{\Gamma}\hat{a}^\dagger(-t)(\hat{\sigma}_{rr} - \hat{\sigma}_{gg}) - \frac{\Omega(t)}{2}e^{i\phi(t)}\hat{\sigma}_{eg}. \quad (\text{E4})$$

Assuming the adiabatic condition, $|\Delta| \gg \Omega(t), \Gamma$, the dynamics of the transition operators involving the excited state are much faster than the rest of the system, therefore, from the perspective of the slowly evolving time scale of the system, the fast-evolving operators reach their steady state, hence we can adiabatically eliminate the excited state $|r\rangle$ by setting $\partial_t\hat{\sigma}_{re} \sim 0$, $\partial_t\hat{\sigma}_{rg} \sim 0$. We arrive at,

$$\hat{\sigma}_{re} \sim [\sqrt{\Gamma}\hat{a}^\dagger(-t)\hat{\sigma}_{ge} + \Omega(t)e^{i\phi(t)}\hat{\sigma}_{ee}/2]/\Delta, \quad (\text{E5})$$

$$\hat{\sigma}_{rg} \sim [\sqrt{\Gamma}\hat{a}^\dagger(-t)\hat{\sigma}_{gg} + \Omega(t)e^{i\phi(t)}\hat{\sigma}_{eg}/2]/\Delta, \quad (\text{E6})$$

where we have used the approximation $\hat{\sigma}_{rr} = \hat{\sigma}_{re}\hat{\sigma}_{er} \sim 1/\Delta^2 \sim 0$. The equation of motion for an system operator \hat{s} between the ground states $|g\rangle$ and $|e\rangle$ is,

$$i\partial_t\hat{s} = \frac{\Omega(t)}{2}(e^{-i\phi(t)}[\hat{s}, \hat{\sigma}_{re}] + e^{i\phi(t)}[\hat{s}, \hat{\sigma}_{er}]) + \sqrt{\Gamma}([\hat{s}, \hat{\sigma}_{rg}]\hat{a}(-t) + \hat{a}^\dagger(-t)[\hat{s}, \hat{\sigma}_{gr}]) \quad (\text{E7})$$

$$= \frac{\Omega(t)}{2}(e^{i\phi(t)}\hat{s}\hat{\sigma}_{er} - e^{-i\phi(t)}\hat{\sigma}_{re}\hat{s}) + \sqrt{\Gamma}(\hat{a}^\dagger(-t)\hat{s}\hat{\sigma}_{gr} - \hat{\sigma}_{rg}\hat{s}\hat{a}(-t)) \quad (\text{E8})$$

$$= \frac{\Gamma}{\Delta}\hat{a}^\dagger(-t)\hat{a}(-t)[\hat{s}, \hat{\sigma}_{gg}] + \frac{\Omega^2(t)}{4\Delta}[\hat{s}, \hat{\sigma}_{ee}] + \frac{\Omega(t)\sqrt{\Gamma}}{2\Delta}e^{i\phi(t)}[\hat{s}, \hat{\sigma}_{eg}]\hat{a}(-t) + \frac{\Omega(t)\sqrt{\Gamma}}{2\Delta}e^{-i\phi(t)}\hat{a}^\dagger(-t)[\hat{s}, \hat{\sigma}_{ge}]. \quad (\text{E9})$$

The equation of motion for the photon field operator is,

$$i\partial_t\hat{a}(x, t) = \sqrt{\Gamma}\hat{\sigma}_{gr}\delta(x + t) \sim \sqrt{\Gamma}\delta(x + t)[\sqrt{\Gamma}\hat{a}(-t)\hat{\sigma}_{gg} + \Omega(t)e^{-x\phi(t)}\hat{\sigma}_{ge}/2]/\Delta. \quad (\text{E10})$$

We then have an effective Hamiltonian describing the dynamics between the ground states and the photon field,

$$\hat{H} = \frac{\Gamma}{\Delta}\hat{\sigma}_{gg}\hat{a}^\dagger(-t)\hat{a}(-t) + \frac{\Omega^2(t)}{4\Delta}\hat{\sigma}_{ee} + \left[\frac{\Omega(t)\sqrt{\Gamma}}{2\Delta}e^{i\phi(t)}\hat{\sigma}_{eg}\hat{a}(-t) + \text{h.c.} \right]. \quad (\text{E11})$$

The first term is the detuning of the photon field followed by two AC Stark shifts of the ground states, the last term is the Jaynes-Cummings-interaction term with an effective time-dependent coupling. Let $\phi(t) = \phi_g(t) + \phi_e(t)$ Going into a rotating frame of the $|e\rangle$ state and choose $\partial_t\phi_e(t) = -\Omega^2(t)/4\Delta$, we recover the effective Hamiltonian given by Eq. (32),

$$\hat{H} = \frac{\Gamma}{\Delta}\hat{\sigma}_{gg}\hat{a}^\dagger(-t)\hat{a}(-t) + \frac{\Omega(t)\sqrt{\Gamma}}{2\Delta}\left[e^{i\phi_g(t)}\hat{\sigma}_{eg}\hat{a}(-t) + \text{h.c.} \right]. \quad (\text{E12})$$

In the following subsections, we carry out the calculations using this effective Hamiltonian.

2. Single excitation

We now provide a derivation of the solution for the time-dependent coupling in the single-excitation limit. We start with the ansatz,

$$|\psi(t)\rangle = \int dx \alpha(x, t) \hat{a}^\dagger(x) |0, g\rangle + \beta(t) |0, e\rangle. \quad (\text{E13})$$

From this, we obtain two equations of motion,

$$i\partial_t \beta(t) = g(t)\alpha(-t, t), \quad (\text{E14})$$

$$i\partial_t \alpha(x, t) = \left[\frac{\Gamma}{\Delta} \alpha(-t, t) + g^*(t)\beta(t) \right] \delta(x + t), \quad (\text{E15})$$

where $g(t) = \frac{\Omega(t)\sqrt{\Gamma}}{2\Delta} e^{i\phi_g(t)}$. Integrating t over the small interval $[x - \epsilon, x + \epsilon]$ on either side of the δ -function to obtain the boundary condition (where we have used $\alpha(-t, t) = [\alpha_0(-t, t) + \alpha_1(-t, t)]/2$ and evaluated $x = -t$)

$$\left(1 - \frac{i\Gamma}{2\Delta}\right) \alpha_0(-t, t) - \left(1 + \frac{i\Gamma}{2\Delta}\right) \alpha_1(-t, t) = ig^*(t)\beta(t). \quad (\text{E16})$$

Substitute the $\alpha_1(-t, t)$ from the boundary condition into the $\beta(t)$ equation we have a Bernoulli equation that governs the dynamics of the $|e\rangle$ state,

$$\partial_t \beta(t) = -\frac{\xi|g(t)|^2}{2} \beta(t) - i\xi g(t)\alpha_0(-t, t), \quad (\text{E17})$$

where we have defined $\xi = [1 + i\Gamma/(2\Delta)]^{-1}$ as a complex factor that is caused by the AC Stark shift in the effective Hamiltonian of Eq. (E12). Notice that from the definition of ξ we have $\text{Re}(\xi) = |\xi|^2$. The Bernoulli equation of $\beta(t)$ has solution

$$\beta(t) = e^{-\xi G(0, t)/2} \left[\beta(0) - i\xi \int_0^t dt' g(t') e^{\xi G(0, t')/2} \alpha_0(-t', t') \right], \quad (\text{E18})$$

where $G(0, t) = \int_0^t dt' |g(t')|^2$. Solving for the release of a single photon in the mode shape $f_{\text{out}}(-t) = \alpha_1(-t, t)$ and $\beta(0) = 1$, $\alpha_0(-t, t) = 0$, from the boundary condition, we need to invert the following equation for $g(t)$

$$f_{\text{out}}(-t) = -i\xi g^*(t) e^{-\xi G(0, t)/2}. \quad (\text{E19})$$

Notice that

$$|f_{\text{out}}(-t)|^2 = |\xi|^2 |g(t)|^2 e^{-\text{Re}(\xi)G(0, t)} = -|\xi|^2 \partial_t e^{-\text{Re}(\xi)G(0, t) / \text{Re}(\xi)} = -\partial_t e^{-|\xi|^2 G(0, t)}, \quad (\text{E20})$$

$$e^{-\text{Re}(\xi)G(0, t)} = 1 - \frac{\text{Re}(\xi)}{|\xi|^2} \int_0^t dt' |f_{\text{out}}(-t')|^2 = \int_t^\infty dt' |f_{\text{out}}(-t')|^2. \quad (\text{E21})$$

We therefore obtain the effective coupling strength for emission,

$$g^*(t) = \frac{if_{\text{out}}(-t)}{\xi \sqrt{\left[\int_t^\infty dt' |f_{\text{out}}(-t')|^2 \right]^{1/\xi}}}. \quad (\text{E22})$$

Similarly, for absorption of a single-photon in the mode shape $f_{\text{in}}(-t) = \alpha_0(-t, t)$ and $\beta(0) = 0$, $\alpha_1(-t, t) = 0$, the boundary condition is of the form of Eq. (24),

$$f_{\text{in}}(-t) = |\xi|^2 g^*(t) e^{-\xi G(0, t)/2} \int_0^t dt' g(t') e^{\xi G(0, t')/2} f_{\text{in}}(-t'). \quad (\text{E23})$$

Whose solution is given by Eq. (25),

$$g^*(t) = \frac{f_{\text{in}}(-t)}{|\xi| \sqrt{\left[\int_0^t dt' |f_{\text{in}}(-t')|^2 \right]^{1/\xi}}}. \quad (\text{E24})$$

These effective couplings can be related to the time-dependent Rabi frequency and phase using the relation.

$$\frac{\Omega(t)}{2} e^{i\phi_g(t)} = \frac{\Delta}{\sqrt{\Gamma}} g(t) e^{-i\frac{\Delta}{\Gamma} G(0, t)} \quad (\text{E25})$$

3. Two excitations

We begin with the two-excitation ansatz,

$$|\psi(t)\rangle_I = \int dx_1 dx_2 \alpha(x_1, x_2, t) \frac{\hat{a}^\dagger(x_1) \hat{a}^\dagger(x_2)}{\sqrt{2}} |0, g\rangle + \int dx \beta(x, t) \hat{a}^\dagger(x) |0, e\rangle. \quad (\text{E26})$$

The equations of motion are,

$$i\partial_t \beta(x, t) = \sqrt{2}g(t)\alpha(x, -t, t) \quad (\text{E27})$$

$$i\partial_t \alpha(x_1, x_2, t) = \left[\frac{\Gamma}{\Delta} \alpha(-t, x_2, t) + \frac{g^*(t)}{\sqrt{2}} \beta(x_2, t) \right] \delta(x_1 + t) + \left[\frac{\Gamma}{\Delta} \alpha(-t, x_1, t) + \frac{g^*(t)}{\sqrt{2}} \beta(x_1, t) \right] \delta(x_2 + t). \quad (\text{E28})$$

where $g(t) = \frac{\Omega(t)\sqrt{\Gamma}}{2\Delta} e^{i\phi_g(t)}$. Like in Sec. II C, we now restrict the wavefunctions to $x_1 \geq x_2$ and split them into the different regions. The boundary conditions are derived by integrating over the δ -functions in Eq. (E28), but due to the AC Stark shift of the ground state, they contain the ξ complex factor,

$$\alpha_0(-t, x_2, t)/\xi^* - \alpha_1(-t, x_2, t)/\xi = \frac{ig^*(t)}{\sqrt{2}} \beta_1(x_2, t), \quad (\text{E29})$$

$$\alpha_1(x_1, -t, t)/\xi^* - \alpha_2(x_1, -t, t)/\xi = \frac{ig^*(t)}{\sqrt{2}} \beta_2(x_1, t). \quad (\text{E30})$$

Substituting $\alpha_1(-t, x_2, t)$ and $\alpha_2(x_1, -t, t)$ from the boundary conditions into the $\beta_1(x_2, t)$ and $\beta_2(x_1, t)$ equations we have the differential equations for the single-photon wavefunctions,

$$\partial_t \beta_1(x_2, t) = -\frac{\xi|g(t)|^2}{2} \beta_1(x_2, t) - i\xi\sqrt{2}g(t)\alpha_0(-t, x_2, t), \quad (\text{E31})$$

$$\partial_t \beta_2(x_1, t) = -\frac{\xi|g(t)|^2}{2} \beta_2(x_1, t) - i\xi\sqrt{2}g(t)\alpha_1(x_1, -t, t). \quad (\text{E32})$$

These Bernoulli equations have solution

$$\beta_1(x_2, t) = e^{-\xi G(0, t)/2} \left[\beta_1(x_2, 0) - i\xi\sqrt{2} \int_0^t dt' g(t') e^{\xi G(0, t')/2} \alpha_0(-t', x_2, t') \right], \quad (\text{E33})$$

$$\beta_2(x_1, t) = e^{-\xi G(-x_1, t)/2} \left[\beta_2(x_1, -x_1) - i\xi\sqrt{2} \int_{-x_1}^t dt' g(t') e^{\xi G(-x_1, t')/2} \alpha_1(x_1, -t', t') \right], \quad (\text{E34})$$

where $G(0, t) = \int_0^t dt' |g(t')|^2$. Here, we can use $\beta_2(x_1, -x_1) = \beta_1(x_1, -x_1)$ and $\alpha_1(x_1, -t, t) = \alpha_1(x_1, -t, -x_1)$, to relate $\beta_2(x_1, t)$ to the initial conditions.

Solving for subtraction, we have the initial state

$$|\psi(t=0)\rangle = \frac{1}{\sqrt{2}} \left[\int dx f_{\text{in}}(x) \hat{a}^\dagger(x) \right]^2 |0, g\rangle. \quad (\text{E35})$$

Ideal subtraction process would require $\alpha_2(x_1, x_2, t) = 0$, and thus the boundary condition becomes $\alpha_1(x_1, -t, t) = i\xi^* g^*(t) \beta_2(x_1, t)/\sqrt{2}$, in terms of the initial conditions, we have

$$\frac{\xi}{\xi^*} f_{\text{in}}(-t) \left[f_{\text{in}}(x_1) - |\xi|^2 g^*(-x_1) e^{-\xi G(0, -x_1)/2} S_{\xi/2}(0, -x_1) \right] \quad (\text{E36})$$

$$= |\xi|^2 g^*(t) e^{-\xi G(-x_1, t)/2} \left\{ e^{-\xi G(0, -x_1)/2} f_{\text{in}}(x_1) S_{\xi/2}(0, -x_1) \right. \quad (\text{E37})$$

$$\left. + \frac{\xi}{\xi^*} S_{\xi/2}(-x_1, t) \left[f_{\text{in}}(x_1) - |\xi|^2 g^*(-x_1) e^{-\xi G(0, -x_1)/2} S_{\xi/2}(0, -x_1) \right] \right\}. \quad (\text{E38})$$

Notice that by setting $\xi = 1$, we recover Eq. (23). Nonetheless, this boundary condition is difficult to solve; hence, we make the linear approximation by setting $-x_1 = t$, the effect is that we are left with a boundary condition that is in the form of Eq. (24),

$$f_{\text{in}}(-t) = \frac{2|\xi|^4}{\xi} g^*(t) e^{-\xi G(0, t)/2} S_{\xi/2}(0, t). \quad (\text{E39})$$

Then the explicit expression for the effective coupling strength is given by Eq. (25),

$$g^*(t) = \frac{f_{\text{in}}(-t)}{\sqrt{2 \text{Re}(\zeta) \left[\int_0^t dt' |f_{\text{in}}(-t')|^2 \right]^{\zeta/\text{Re}(\zeta)}}}, \quad (\text{E40})$$

with $\zeta = \frac{2|\xi|^4}{\xi} - \frac{\xi}{2}$.

4. Linearised n -excitation subtraction

We now generalise the two-excitation ansatz to the n -excitation problem. The derivation in this subsection is similar to Appendix C, we shall skip most of the detail and only present important steps. The ansatz for the n -excitation subspace is identical to that of Eq. (C1). From the Schrödinger equation, the equations of motion are

$$i\partial_t \alpha(\mathbf{x}, t) = \sum_{j=1}^n \delta(x_j + t) \left[\frac{g^*(t)}{\sqrt{n}} \beta(\mathbf{x}, t) + \frac{\Gamma}{\Delta} \alpha(\mathbf{x}, t) \Big|_{x_j = -t} \right], \quad (\text{E41})$$

$$i\partial_t \beta(\mathbf{x}, t) = \sqrt{n} g(t) \alpha(\mathbf{x}, t) \Big|_{x_m = -t}. \quad (\text{E42})$$

Similar to Eq. (C4), the boundary conditions are,

$$\frac{\alpha_m(\mathbf{x}, t)}{\xi} \Big|_{x_m = -t} - \frac{\alpha_{m-1}(\mathbf{x}, t)}{\xi^*} \Big|_{x_m = -t} = -i \frac{g^*(t)}{\sqrt{n}} \beta_m(\mathbf{x}, t), \quad (\text{E43})$$

where $m = 0, 1, \dots, n-1$. Together with the regularisation condition and the above boundary conditions, Eq. (E42) produces n differential equations,

$$\partial_t \beta_m(\mathbf{x}, t) = -\frac{\xi |g(t)|^2}{2} \beta_m(\mathbf{x}, t) - i\xi \sqrt{n} g(t) \alpha_{m-1}(\mathbf{x}, t) \Big|_{x_m = -t}, \quad (\text{E44})$$

each with domain $-t \in [x_{m-1}, x_m]$ with $x_0 = 0$.

We solve the n -excitation subtraction process with $\alpha_0(\mathbf{x}, 0) = \alpha_0(\mathbf{x}, t) = \prod_{j=1}^n f_{\text{in}}(x_j)$. Solving Eq. (E44) for $\beta_1(\mathbf{x}, t)$ gives

$$\beta_1(\mathbf{x}, t) = -i\xi \sqrt{n} \prod_{j=2}^n f_{\text{in}}(x_j) e^{-\xi G(0,t)/2} S_{\xi/2}(0, t), \quad (\text{E45})$$

From the boundary condition in Eq. (E43), we can relate $\alpha_1(\mathbf{x}, t)$ to the initial conditions by

$$\alpha_1(\mathbf{x}, t) \Big|_{x_1 = -t} = \frac{\xi}{\xi^*} \prod_{j=2}^n f_{\text{in}}(x_j) \left[f_{\text{in}}(-t) - |\xi|^2 g^*(t) e^{-\xi G(0,t)/2} S_{\xi/2}(0, t) \right]. \quad (\text{E46})$$

Since Eq. (E42) does not contain any δ -functions, we have the matching boundary condition for the $(n-1)$ -photon wavefunctions, $\beta_m(\mathbf{x}, t)|_{x_{m-1} = -t} = \beta_{m-1}(\mathbf{x}, t)|_{x_m = -t}$. Combined with the boundary condition in Eq. (E43), this allows us to relate the n -photon in arbitrary regions to the initial conditions, provided we evaluate the position coordinates appropriately,

$$\frac{1}{\xi} \alpha_m(\mathbf{x}, t) \Big|_{x_{1:m} = -t} - \frac{1}{\xi^*} \alpha_{m-1}(\mathbf{x}, t) \Big|_{x_{1:m} = -t} = -i \frac{g^*(t)}{\sqrt{n}} \beta_m(\mathbf{x}, t) \Big|_{x_{1:m-1} = -t} = -i \frac{g^*(t)}{\sqrt{n}} \beta_1(\mathbf{x}, t) \Big|_{x_{2:m} = -t}. \quad (\text{E47})$$

By induction, one can relate the n -photon wavefunction with label m to the initial conditions with the appropriate linearisations,

$$\alpha_m(\mathbf{x}, t)|_{x_{1:m} = -t} = \prod_{j=m+1}^n f_{\text{in}}(x_j) f_{\text{in}}^{m-1}(-t) \left[\left(\frac{\xi}{\xi^*} \right)^m f_{\text{in}}(-t) - \sum_{k=1}^m \left(\frac{\xi}{\xi^*} \right)^k |\xi|^2 g^*(t) e^{-\xi G(0,t)/2} S_{\xi/2}(0, t) \right]. \quad (\text{E48})$$

We prove the above closed form by induction. Since $\alpha_0(\mathbf{x}, t)$ and $\alpha_1(\mathbf{x}, t)|_{x_1=-t}$ are already in the closed form. From the linearised boundary condition given by Eq. (E47) and applying the induction step we have,

$$\alpha_{m+1}(\mathbf{x}, t)|_{x_{1:m+1}=-t} = \frac{\xi}{\xi^*} \alpha_m(\mathbf{x}, t) \Big|_{x_{1:m+1}=-t} - \frac{i\xi g^*(t)}{\sqrt{n}} \beta_1(\mathbf{x}, t) \Big|_{x_{2:m+1}=-t} \quad (\text{E49})$$

$$\begin{aligned} &= \frac{\xi}{\xi^*} \prod_{j=m+2}^n f_{\text{in}}(x_j) f_{\text{in}}^m(-t) \left[\left(\frac{\xi}{\xi^*} \right)^m f_{\text{in}}(-t) - \sum_{k=1}^m \left(\frac{\xi}{\xi^*} \right)^k |\xi|^2 g^*(t) e^{-\xi G(0,t)/2} S_{\xi/2}(0, t) \right] \\ &\quad - \frac{\xi}{\xi^*} |\xi|^2 \prod_{j=m+2}^n f_{\text{in}}(x_j) f_{\text{in}}^m(-t) g^*(t) e^{-\xi G(0,t)/2} S_{\xi/2}(0, t) \end{aligned} \quad (\text{E50})$$

$$= \prod_{j=m+2}^n f_{\text{in}}(x_j) f_{\text{in}}^m(-t) \left[\left(\frac{\xi}{\xi^*} \right)^{m+1} f_{\text{in}}(-t) - \sum_{k=1}^{m+1} \left(\frac{\xi}{\xi^*} \right)^k |\xi|^2 g^*(t) e^{-\xi G(0,t)/2} S_{\xi/2}(0, t) \right], \quad (\text{E51})$$

as required.

Finally, the output boundary condition for the ideal subtraction process requires $\alpha_n(\mathbf{x}, t) = 0$, together with the linear approximation, the output boundary condition is $\alpha_{n-1}(\mathbf{x}, t)|_{x_{1:n}=-t}/\xi^* = ig^*(t)\beta_1(\mathbf{x}, t)|_{x_{2:n}=-t}/\sqrt{n}$. In terms of the initial conditions,

$$\begin{aligned} &\left(\frac{\xi}{\xi^*} \right) f_{\text{in}}^{n-1}(-t) \left[\left(\frac{\xi}{\xi^*} \right)^{n-1} f_{\text{in}}(-t) - \sum_{k=1}^{n-1} \left(\frac{\xi}{\xi^*} \right)^k |\xi|^2 g^*(t) e^{-\xi G(0,t)/2} \phi_\xi(0, t) \right] \\ &= f_{\text{in}}^{n-1}(-t) \frac{\xi}{\xi^*} |\xi|^2 g^*(t) e^{-\xi G(0,t)/2} S_{\xi/2}(0, t) \end{aligned} \quad (\text{E52})$$

$$f_{\text{in}}(-t) = \frac{1 - (\xi^*/\xi)^n}{1 - \xi^*/\xi} |\xi|^2 g^*(t) e^{-\xi G(0,t)/2} S_{\xi/2}(0, t). \quad (\text{E53})$$

Recongize that the above boundary condition is in the form of Eq. (24), then the dynamic coupling is

$$g^*(t) = \frac{f_{\text{in}}(-t)}{\sqrt{2 \operatorname{Re}(\zeta) \left[\int_0^t dt' |f_{\text{in}}(-t')|^2 \right]^{\zeta/\operatorname{Re}(\zeta)}}}, \quad (\text{E54})$$

with $\zeta = \frac{1 - (\xi^*/\xi)^n}{1 - \xi^*/\xi} |\xi|^2 - \frac{\xi}{2}$.